



## Fecundity, *in vitro* early larval development and karyotype of the zoonotic nematode *Anisakis pegreffii*

Samantha Moratal<sup>a,b,\*</sup>, Magda Zrzavá<sup>c,d</sup>, Jerko Hrabar<sup>e</sup>, María Auxiliadora Dea-Ayuela<sup>f</sup>, Jordi López-Ramon<sup>b,g</sup>, Ivona Mladineo<sup>a</sup>

<sup>a</sup> Laboratory of Functional Helminthology, Institute of Parasitology, Biology Centre Czech Academy of Sciences, Branišovská 1160/31, 37005 České Budějovice, Czechia

<sup>b</sup> Servicio de Análisis, Investigación y Gestión de Animales Silvestres (SAIGAS), Facultad de Veterinaria, Universidad Cardenal Herrera-CEU, CEU Universities, C/ Tirant lo Blanc, Alfara del Patriarca, 46115 Valencia, Spain

<sup>c</sup> Faculty of Science, University of South Bohemia, Branišovská 1760/31a, 37005, České Budějovice, Czechia

<sup>d</sup> Institute of Entomology, Biology Centre Czech Academy of Sciences, Branišovská 1160/31, 37005, České Budějovice, Czechia

<sup>e</sup> Laboratory of Aquaculture, Institute of Oceanography and Fisheries, 21000 Split, Croatia

<sup>f</sup> Departamento de Farmacia, Facultad de Ciencias de la Salud, Universidad Cardenal Herrera-CEU, CEU Universities, C/ Santiago Ramón y Cajal, Alfara del Patriarca, 46115 Valencia, Spain

<sup>g</sup> Wildlife Ecology & Health Group (WE&H), Facultad de Veterinaria, Universitat Autònoma de Barcelona (UAB), Travessera dels Turons, Bellaterra, 08193 Barcelona, Spain

### ARTICLE INFO

#### Keywords:

*Anisakis pegreffii*  
*Anisakis simplex*  
 Fecundity  
*in vitro*  
 Karyotype  
 Ultrastructure

### ABSTRACT

The *in vitro* life cycle of zoonotic helminths is an essential tool for -omic translational studies focused on disease control and treatment. Anisakiosis is an emerging zoonosis contracted by the ingestion of raw or undercooked fish infected with the third stage larvae (L3) of two sibling species *Anisakis simplex* sensu stricto (s.s.) and *Anisakis pegreffii*, the latter being the predominant species in the Mediterranean basin. Recently, *in vitro* culture of *A. pegreffii* has been developed to enable fast and large-scale production of fertile adults. However, the conditions for larval development from hatching to infective L3 were not fulfilled to complete the cycle. Herein, we used a *Drosophila* medium supplemented with chicken serum and adjusted different osmolarities to maintain the culture of L3 hatched from eggs for up to 17 weeks. The highest survival rate was observed in the medium with the highest osmolarities, which also allowed the highest larval exsheathment rate. Key morphological features of embryogenesis and postembryogenesis studied by transmission electron microscopy revealed that the excretory gland cell is differentiated already up to 48 h post-hatching. Extracellular vesicles and cell-free mitochondria are discharged between the two cuticle sheets of the second stage larvae (L2). Contemporarily cultivated, two populations of adult *A. simplex* s.s. and *A. pegreffii* reached an average production of 29,914.05 ( $\pm$  27,629.36) and 24,370.96 ( $\pm$  12,564.86) eggs/day/female, respectively. The chromosome spreads of *A. pegreffii* obtained from mature gonads suggests a diploid karyotype formula of  $2n = 18$ . The development of a reliable protocol for the *in vitro* culture of a polyxenous nematode such as *Anisakis* spp. will serve to screen for much needed novel drug targets, but also to study the intricate and unknown ecological and physiological traits of these trophically transmitted marine nematodes.

### 1. Introduction

Research of fundamental mechanisms of helminth function, survival and reproduction has been incentivised by the pioneering use of -omics tools, enabling major steps in translating existing knowledge in measures to mitigate and control of highly prevalent neglected diseases

(International Helminth Genomes Consortium, 2019; Jasmer et al., 2019). While relying on environmental and clinical samples of helminths as a source for downstream -omics protocols is practical and fitting for the variety of experimental hypotheses, other protocols may require higher numbers of developmental stages that are not always available in nature, or clonal and less heterogeneous parasite

\* Corresponding author at: Servicio de Análisis, Investigación y Gestión de Animales Silvestres (SAIGAS), Facultad de Veterinaria, Universidad Cardenal Herrera-CEU, CEU Universities, C/ Tirant lo Blanc, Alfara del Patriarca, 46115 Valencia, Spain.

E-mail address: [samantha.moratal@gmail.com](mailto:samantha.moratal@gmail.com) (S. Moratal).

<https://doi.org/10.1016/j.vetpar.2023.110050>

Received 11 June 2023; Received in revised form 27 September 2023; Accepted 7 October 2023

Available online 12 October 2023

0304-4017/© 2023 The Author(s). Published by Elsevier B.V. This is an open access article under the CC BY-NC license (<http://creativecommons.org/licenses/by-nc/4.0/>).

populations grown under specific conditions, especially in cases where gene functions are explored through gene editing techniques (Gang et al., 2020; Cheong et al., 2021). Therefore, *in vitro* life cycle protocols for helminths, especially zoonotic taxa, represent a fundamental tool providing ideal conditions for rearing parasites in large numbers, repeatability and a reliable environment for comparing mechanisms in wild-type specimens. However, even the number of known natural life cycles of trophically transmitted helminths is considerably small (i.e., 973) relative to the number of host-parasite-species associations (Benesh et al., 2017). This results in knowledge gaps that prevent us from fully understanding helminth co-evolution and infection and evasion strategies - important variables to consider in parasitosis management.

Anisakiosis is an emerging zoonosis caused by the sibling species *Anisakis simplex* sensu stricto (s.s.) and *Anisakis pegreffii* (Anisakidae) (Adroher-Auroux and Benítez-Rodríguez, 2020) contracted through the consumption of raw or inadequately processed fish infected with third stage (L3) nematode larvae. The disease is usually associated with an acute gastrointestinal or gastro-allergic reaction (Daschner and Pascual, 2005; Audicana and Kennedy, 2008), which has been known for a long time (i.e., the first observation was reported in 1876 (Leuckart, 1876)) but remains misdiagnosed, under-reported and unknown in countries with below-average fish consumption. In contrast, reports suggest that the number of cases is increasing in proportion to changes in food consumption habits worldwide (European Food Safety Authority (EFSA) Panel on Biological Hazards (BIOHAZ), 2010; Llarena-Reino et al., 2015), resulting in anisakiosis ranking fifth in the European risk classification and being the second of 24 foodborne parasitoses with the highest “increasing illness potential” (Bouwknegt et al., 2018).

Recently, a reliable protocol for *in vitro* culture of *A. pegreffii* has been established, allowing adult development, harvest of fertilised eggs and hatching of second stage (L2) larvae (Mladineo et al., 2023). However, no further development towards the later larval or adult stages was followed in the study, which would help to elucidate certain aspects of the biology of the species. In the marine environment, hatched and free-swimming L2 are preyed upon by crustaceans (mainly euphausiids) and possibly small fish (Aibinu et al., 2019). L2 are thought to grow in the crustacean haemocoel after ingestion and moult into L3 (Smith, 1983), although the specific conditions and cues required for this process are as yet unknown. Of particular interest is the development of the excretory gland cell (EGC). This conspicuous cell is considered the main production site for the excretory/secretory products (ESPs) and extracellular vesicles (EVs) of anisakids (Cavallero et al., 2018; Mladineo et al., 2023) and is thus a *conditio sine qua non* for efficient virulence and propagation of the nematode. ESPs and EVs secreted by L3 contribute to the activation of kinases involved in inflammation and cell proliferation (or inhibition of apoptosis) (Messina et al., 2016), as well as to processes supporting inflammation, apoptosis, cell proliferation and differentiation, respectively (Cavallero et al., 2022). Thus, the ontogeny of EGC through earlier stages could provide valuable insights into the host-parasite interaction of anisakids, which is particularly interesting from a co-evolutionary aspect of a parasite inhabiting multiple hosts.

The main objective of this study was to test the conditions for *in vitro* development of L3 stages from *A. pegreffii* eggs and to determine the morphological characteristics of early L2 larvae using transmission electron microscopy (TEM). Furthermore, capitalising on two adult populations maintained *in vitro*, i.e., *A. pegreffii* from the Adriatic Sea and a mixed *A. simplex* sensu lato (s.l.) population from the east coast of the North Atlantic, we monitored and compared fecundity over time, thus obtaining the first long-term data on the fecundity of anisakids *in vitro*. Finally, we obtained the first chromosome spreads of *A. pegreffii* and defined the karyotype of the species, which may be a valuable tool for molecular cytological studies in the future and contribute to better genome assembly and chromosome mapping (Doyle, 2022).

## 2. Materials and methods

### 2.1. Origin of *Anisakis* spp. third stage larvae (L3)

*Anisakis* spp. type I larvae were collected from naturally infected blue whiting *Micromesistius poutassou* acquired from commercial fishermen in two different locations: Adriatic Sea (Croatia, FAO Division 37.2.1) and North Atlantic (Spain, FAO Division 27.8). Fish were stored on ice until dissection at the Institute of Oceanography and Fisheries, Croatia (Adriatic population) and at the Faculty of Health Sciences from University Cardenal Herrera-CEU, Spain (North Atlantic population). The actively moving L3 were removed from the viscera and visceral cavity with small forceps, washed with physiological saline, placed in 50 mL tubes containing autoclaved seawater and shipped to the Institute of Parasitology in the Czech Republic. Immediately after arrival, larvae were washed in autoclaved M9 buffer containing 2% penicillin/streptomycin (PS) (Sigma, P4333–20 mL) and amphotericin B (Sigma, A2942–20 mL) (three 30-min washes at room temperature and protected from light). Finally, larvae were examined under a stereomicroscope (Zeiss, Stemi 305) for morphological genus confirmation and integrity.

### 2.2. *In vitro* culture and eggs harvesting

L3 larvae were cultured in autoclaved glass bottles (one batch for the Adriatic population and one batch for the North Atlantic population) to reach the adult stage, according to the protocol recently established by Mladineo et al. (2023).

After observing the first eggs expelled in the medium in the 3rd week in culture, the eggs were collected for subsequent quantification each time the medium was changed (three times per week). This means that the eggs expelled were produced over 48 h (if collected on Wednesdays and Fridays) or 72 h (if collected on Mondays). The medium was collected in 50 mL tubes and centrifuged at 22xg for 20 min at 19 °C. After discarding the supernatant, the pellet was washed twice in 5 mL of autoclaved sea salt solution (SSS) [31.73 g of Sea salts NutriSelect Basic (Sigma, S9883–500 G) in 1 L of distilled water] by centrifugation under the previous conditions. The eggs were resuspended in autoclaved SSS and filtered through a 70 µm pore size nylon cell strainer (Corning, 734–2761). After another centrifugation cycle, the supernatant was discarded and eggs were resuspended in 1–3 mL of SSS, depending on the number of eggs (more SSS for a larger egg pellet). The resuspension was thoroughly mixed by pipetting and used to fill a Bürker chamber. Quantification was performed under the light microscope (Olympus, CKX53) according to the standard protocol for blood cell counting in the Bürker chamber:

$$\text{Eggs/mL} = (\text{Total eggs counted} \times 10,000 \text{ eggs/mL}) / \text{Number of squares counted}$$

$$\text{Total eggs/medium} = \text{Total eggs/mL} \times \text{Volume of sample containing the eggs}$$

In addition, the number and sex of the dead adult specimens were noted at each egg harvesting.

Eggs for L2 culture were collected following the same protocol with few modifications. After changing the medium on a given day, the adults were left in the new medium for a maximum of 4 h. Eggs were then collected to ensure that only recently expelled eggs were harvested and to minimise the potentially deleterious effect of the acidic culture medium on the eggs. Eggs were centrifuged and washed twice in complete SSS; autoclaved SSS containing 2% PS and nystatin (1 mL/L) (Sigma, N9150–20 mL). The pellet was resuspended in 1–3 mL of complete SSS, passed through a cell strainer to remove cell debris, and the filtrate was divided into 50–100 µL aliquots in 6 well plates. A further 2 mL of complete SSS were added and the eggs were incubated at 19 °C in a 5% CO<sub>2</sub> atmosphere. Under these conditions, the first L2 hatched on day five (6–7 days for the early egg batches) and were left for a further 48 h due

to asynchronous hatching. 48 h after hatching, the larvae were separated from the unfertilised and unhatched eggs with a 30 µm mesh cell strainer (pluriStrainer® S/ 30 µm, pluriSelect) and collected in a Petri dish for subsequent culture testing.

### 2.3. Fecundity

The fecundity was expressed as the number of eggs expelled per day in *A. pegreffii* and *A. simplex* s.l. colonies. At the same time, we recorded the number, sex and date of adults removed from the culture (due to other sampling requirements and mortality). Using the total number of adults initially placed in the culture and the calculated sex ratio (expressed as a percentage of females) at each count, we plotted the number of eggs per day and per reproductive female. Day 0 corresponds to the day when the L3 were placed in culture to obtain the adults. Fertility (here considered as the percentage of hatched L2 out of a total number of eggs collected) was not assessed quantitatively, but we recorded the time point at which fertilisation of eggs started and stopped.

### 2.4. Culture of *A. pegreffii* L2, survival and exsheathment rate

Culture of *A. pegreffii* L2 obtained *in vitro* was performed in commercial Schneider's *Drosophila* Medium (SDM) (Gibco, 21720024) supplemented with 1% sodium pyruvate (Sigma, S8636–100 mL), 5 µg/mL liver concentrate (Sigma, 2023–50 G), 10% chicken serum (CS) (Merck, C5405–100 mL), 2% PS and 1 mL/L nystatin. The complete medium (pH ≈7 and osmolarity ≈300 mOsm) was syringe filtered (0.22 µm, Techno Plastic Products, 99722) before use.

By manual micropipetting (100 µL tips), 10 harvested L2 no older than 48 h were redistributed into a 24-well plate containing SDM (19 °C; 500 µL/well) prepared at different osmolarities (300, 400, 500, 600, 700, 800 mOsm) and in SSS + SDM (1:1), each in duplicate. The change in osmolarity was adjusted by adding 5 M NaCl directly to the wells containing the medium and gently stirring the plate. Larvae in SSS were considered as controls. The plate containing L2 was incubated at 19 °C in a 5% CO<sub>2</sub> atmosphere.

Preliminary tests showed that although L2 grew in Dulbecco's modified Eagle's medium-low glucose and -high glucose and in SDM for at least two weeks, survival was higher in the latter, as was L2 size, when 20–50% CS was added (Mladineo et al., 2023). We selected lower CS concentration (10%) to allow balanced growth and stable exsheathing processes. Based on the observation that crustaceans and thus anisakids do not thrive in low salinity environments (e.g., brackish water), different osmolarities were tested. However, the osmolarity values in the haemocoel of crustaceans where L2 moults into L3 are also variable and depend on the crustacean species, moulting cycle, body weight or nutritional status (Van Mai and Fotedar, 2018).

The larvae were checked daily under the microscope (Olympus, CKX53) and the medium was partially replaced once a week by surface aspiration. The experiment was terminated at week 11 when less than 15% of the larvae were still alive. The remaining larvae were pooled in two wells with culture medium at 700 mOsm: one well contained the "small L3 phenotype" and the other the "large L3 phenotype". These larvae were kept in culture for further microscopy, the last four surviving until week 17.

Larval survival, number of exsheathed larvae and observation of large L3 phenotypes were recorded three times per week and plotted in ggplot2 package (Wickham, 2016) for R (R version 4.1.2; R Core Team, 2021). To test the effect of osmolarity on survival and exsheathment frequency, pairwise comparisons were performed using Fisher's exact test with Benjamini-Hochberg FDR correction method using R software (R core Team, 2021) and rstatix package (Kassambara, 2023). Significance was set at a P-value of less than 0.05.

## 2.5. Morphological characterization of *A. pegreffii* early developmental stages

### 2.5.1. Morphometry

Samples of recently expelled eggs (<24 h; N = 35), embryonated eggs before hatching (6 days incubation, N = 30), recently hatched larvae (<48 h, N = 25), un-exsheathed larvae cultured for 3 weeks (N = 16) and exsheathed larvae (N = 7) were either fixed with paraformaldehyde 4% or left in SSS to be examined under contrast phase microscope (Olympus BX63F with camera DP74). Measurements were performed using cellSens Dimension Desktop 2.2 with the CI Deconvolution package and images were assembled and annotated in Inkscape 1.0 software (<https://inkscape.org>).

### 2.5.2. Transmission electron microscopy (TEM)

Recently expelled eggs (<24 h), embryonated eggs before hatching (6 days incubation) and recently hatched larvae (<48 h) were used for TEM study. Eggs and larvae were transferred to 1.5 mL tubes in autoclaved SSS and centrifuged at 60xg for 5 min. The supernatant was discarded and the pellet containing the eggs/larvae was transferred to 0.2 mL PCR microtubes. After centrifugation (5 min, 60xg), the eggs/larvae were collected from the pellet using cellulose capillary tubes with an inner diameter of 200 µm, fibre length of 50 mm and wall thickness of 8 µm (LEICA, 16706869), which were immediately processed for high-pressure freezing and freeze substitution as described in Mladineo et al. (2023). Briefly, samples were washed in acetone (3 ×15 min each) and infiltrated in 25%, 50% and 75% mixtures of low viscosity Spurr resin (SPI Chem, West Chester, PA, USA) and anhydrous acetone for 1 h each, and left overnight in 100% resin. The samples were then placed in embedding moulds for polymerisation (48 h at 60 °C). Semi-thin sections (0.5 µm) stained with toluidine blue (1%) were checked for orientation under the light microscope. Ultrathin sections (0.07 µm) were mounted on Formvar-coated single-slot grids and contrasted in ethanolic uranyl acetate (30 min) and lead citrate (20 min) before observation under a JEOL JEM-1400 microscope (JEOL, Akishima, Tokyo, Japan) operating at an accelerating voltage of 120 kV. The images were taken with a XAROSA 20-megapixel CMOS camera (EMSIS GmbH) and assembled and annotated in Inkscape 1.0 software (<https://inkscape.org>).

## 2.6. *A. pegreffii* karyotype

### 2.6.1. Chromosome preparations

Ten adult *A. pegreffii* obtained *in vitro* were used to prepare chromosome spreads (5 males and 5 females; 6–11 weeks old). Specimens were dissected in physiological solution (Glaser, 1917) under a stereomicroscope (Zeiss, Stemi 305) and the gonadal tissues was immediately placed in hypotonic solution (0.075 M KCl) for 5 min. Tissues were then transferred to freshly prepared Carnoy's fixative (6:3:1; ethanol - chloroform - acetic acid) for 10–15 min. After fixation, a very small piece of tissues (1–5 mm long) was transferred onto a superfrost slide (previously washed for one hour in acidic ethanol [0.5 mL HCl + 50 mL 99% EtOH]) in a 10 µL drop of 60% acetic acid and torn into fine fragments using two tungsten needles. The slide was then heated on a hot plate at 45 °C and the drop of acetic acid was moved with a tungsten needle in an area of less than 24 × 40 mm until the liquid evaporated. Finally, the slide was dehydrated through an ascending ethyl alcohol series (70%, 80%, 99%; 60 s each) and air dried. A Jenalumar phase contrast microscope (Carl Zeiss Jena, Germany) was used to check the quality of the spreads before DAPI (4',6-diamidino-2-phenylindole) staining or fluorescence *in situ* hybridisation (FISH).

### 2.6.2. DAPI staining and FISH with biotin-labelled telomeric probe

Part of the slides were stained directly by adding a drop of Fluoroshield™ with DAPI (Sigma, F6057–20 mL) and covered with a coverslip. The rest of the slides were frozen and later used for FISH of nematode telomeric sequence.

The telomeric nematode probe (TTAGGC)<sub>n</sub> was synthesised by the non-template PCR method (following Sahara et al., 1999) and labelled with biotin-16-dUTP by nick translation using the Biotin16 NT Labeling Kit (PP-310 L-BIO16, Jena Bioscience) according to the manufacturer's instructions.

We used the FISH procedure, combining hybridization described in Sahara et al. (1999) with the post-hybridisation washing and detection procedures described in Cabral de Mello and Marec (2021). Briefly, the hybridisation mixture contained 50 ng of the biotin-labelled probe, 25 µg of sonicated salmon sperm DNA (Sigma Aldrich, St. Louis, MO, USA), 50% deionised formamide, 10% dextran sulphate and 2x saline sodium citrate buffer (SSC). Chromosome slides were removed from the freezer, passed through the ethanol series (70%, 80% and 100%, 30 s each) and air dried. The slides were then denatured in 70% deionised formamide in 2 x SSC for 3 min 30 s at 68 °C, incubated in cold 70% ethanol (-20 °C, 1 min), passed through 80% and 100% ethanol and air dried. The hybridisation mixture was denatured at 90 °C for 5 min, immediately cooled on ice and applied to the denatured slide. Hybridisation took place overnight at 37 °C. Washes after hybridisation were as follows: twice in 2 x SSC at 42 °C for 5 min, twice in 0.1 x SSC at 42 °C for 5 min, once in 2 x SSC for 5 min at 42 °C, once in 2 x SSC in a Coplin jar for 10 min at RT, incubation in WBB (4 x SSC, 0.1% v/v Tween 20, 1% w/v skimmed milk) in a Coplin jar for 15 min at RT. Probe detection was performed with streptavidin-Cy3 (Jackson ImmunoRes. Labs. Inc., West Grove, PA, USA) in WBB for 1 h at 37 °C. Then the slide was washed three times in WBB in a Coplin jar for 5 min each at 45 °C and mounted in DAPI (c = 1 µg/mL) in DABCO antifade.

### 2.6.3. Microscopy and image processing

DAPI and FISH slides were observed under confocal and fluorescence microscopes (Olympus FV 3000 and Zeiss Axioplan 2 microscope (Carl Zeiss, Jena, Germany), respectively). For FISH slides, black and white images were taken separately for each fluorescent dye and later pseudo-coloured (red for Cy3 and light blue for DAPI) and merged using Adobe Photoshop CS6 (Adobe Systems, San Jose, CA, USA).

### 2.7. Molecular identification

A subsample of 32 adult nematodes from *in vitro* culture was used for molecular identification of *Anisakis* spp., comprising 15 and 17 individuals from the North Atlantic and Adriatic batches, respectively. DNA was extracted using the SSTNE buffer and salt precipitation as previously described (Bartie et al., 2020). A ~600 bp fragment of cytochrome oxidase subunit 2 (*cox2*) was amplified by combining 50 ng of purified DNA, 12.5 µL Premix Ex Taq Hot Start Version (Takara, Shiga, Japan), 0.5 µL (0.2 mM) of each primer, forward 211 F 5'- TTT TCT AGT TAT ATA GAT TGR TTYAT - 3' and reverse 210 R 5'- CAC CAA CTC TTA AAA TTA C-3' (Nadler and Hudspeth, 2000), and nuclease-free water to a volume of 25 µL. Cycling conditions were set as follows: 30 cycles for 10 s at 98 °C, 30 s at 46 °C (annealing) and 1 min at 72 °C. PCR products were visualised in a 1% agarose gel stained with SYBR™ Safe (Invitrogen, Waltham, MA, USA) and commercially sequenced (Macrogen Europe Laboratory, The Netherlands). The sequences obtained were aligned with the sequences of *Anisakis* spp. available in GenBank (<https://www.ncbi.nlm.nih.gov/genbank/>) (*A. simplex* s.s. (DQ116426), *A. pegreffii* (DQ116428.1), *Anisakis berlandi* (DQ116429.1), *Anisakis ziphidarum* (DQ116430.1), *Anisakis typica* (DQ116427.1), *Anisakis nascettii* (DQ116431.1), *Anisakis physeteris* (DQ116432.1), *Anisakis paggiae* (DQ116434.1), *Anisakis brevispiculata* (DQ116433.10029)) by the Clustal W algorithm implemented in the Mega X software (Kumar et al., 2018), checked for incorrectly read bases and manually corrected if necessary. Species were identified by comparing the sequences with those available in GenBank using BLASTn (Altschul et al., 1990). Sequences were deposited in GenBank with accession numbers OQ919751-OQ919762 for *A. simplex* and OQ919763-OQ919782 for *A. pegreffii*. Bayesian inference analysis was

performed in MrBayes 3.2.7 (Ronquist et al., 2012) to discriminate between specimens of *A. simplex* s.s. and *A. pegreffii* (Supplementary Fig. S1).

The same samples were additionally genotyped using PCR-based restriction fragment length polymorphism (PCR-RFLP) to discern potential recombinant (hybrid) genotypes. Samples were amplified as described above with forward primer BD1 5'- GTC GTA ACA AGG TTT CCG TA - 3' and reverse primer BD2 5'- TAT GCT TAA ATT CAG CGG GT - 3' at the locus of the internal transcribed space region (*ITS*) of the rDNA. Cycling conditions were the same as above except that the annealing temperature was set to 56 °C. Successfully amplified samples were digested with 5 U *HinfI* endonuclease (Promega, Madison, WI, USA) and visualised in 2% agarose gel. Species were identified using the RFLP pattern according to D'Amelio et al. (2000).

## 3. Results

### 3.1. Molecular identification

Based on the BLASTn results for the 584 bp long *cox2* sequences, 12 specimens (37.5%) were identified as *A. simplex* (all of them originating from the North Atlantic batch), and 20 specimens were identified as *A. pegreffii* (17 specimens originating from the Adriatic batch and three specimens from the North Atlantic batch), showing 99.14–100% and 99.83–100% identity with the sequences deposited in GenBank, respectively. The identity of the species was also confirmed by phylogenetic relationship reconstruction. The Bayesian inference consensus tree clustered the 12 identified *A. simplex* specimens with the respective reference sequence, while 20 *A. pegreffii* specimens were clustered with the respective *A. pegreffii* reference sequence (Supplementary Fig. S1).

PCR-based restriction fragment length polymorphism with *HinfI* revealed three distinct patterns: i) three fragments of approximately 370 bp, 300 bp and 250 bp corresponding to *A. pegreffii*; ii) two fragments of approximately 620 bp and 250 bp corresponding to *A. simplex*; iii) four fragments of approximately 620 bp, 370 bp, 300 bp and 250 bp corresponding to the recombinant genotype (putative hybrid). Based on the RFLP pattern, 12 (37.5%) specimens were identified as *A. simplex*, 18 specimens (56.25%) were identified as *A. pegreffii* and two specimens (6.25%) were assigned recombinant genotypes. Both specimens with recombinant genotypes at the *ITS* locus had *A. pegreffii* matrilineage.

### 3.2. Fecundity

The batch of *A. pegreffii* consisted of 57 individuals, with the sex ratio, i.e., the percentage of females, ranging from 37.50% to 40% (variable at different times due to mortality or sampling of specimens for other protocols). The first eggs were detected on day 21, albeit in very small numbers. Fig. 1 shows the number of eggs per day per female, starting from day 25 until the end of the experiment (day 120). The experiment was terminated due to increased adult mortality and probable fungal contamination from dead specimens, although egg production did not decrease at this time. Average production was 24,370.96 ± 12,564.86 eggs/day/female (mean ± standard deviation), with a minimum and maximum of 1562.79 and 43,007.75 eggs/day/female, respectively. Fertilised eggs were present from day 31 to day 86, although fertility was not quantitatively assessed. Hatching of embryonated eggs occurred between days 5–7.

Fifty individuals formed *A. simplex* batch, with sex ratios ranging from 51.06% to 69.23% throughout the experiment. Similar to *A. pegreffii*, the first eggs were detected on day 24. The number of eggs per day per female is shown in Fig. 1, from day 27 until the end of the experiment (day 162). In this case, the experiment was terminated when < 5 worms remained (extractions mainly due to sampling). The average, minimum and maximum egg production was 29,914.05 ± 27,629.36, 713.58 and 115,694.45 eggs/day/female, respectively. Fertilised eggs were present at least between days 64 and 108, and also hatched

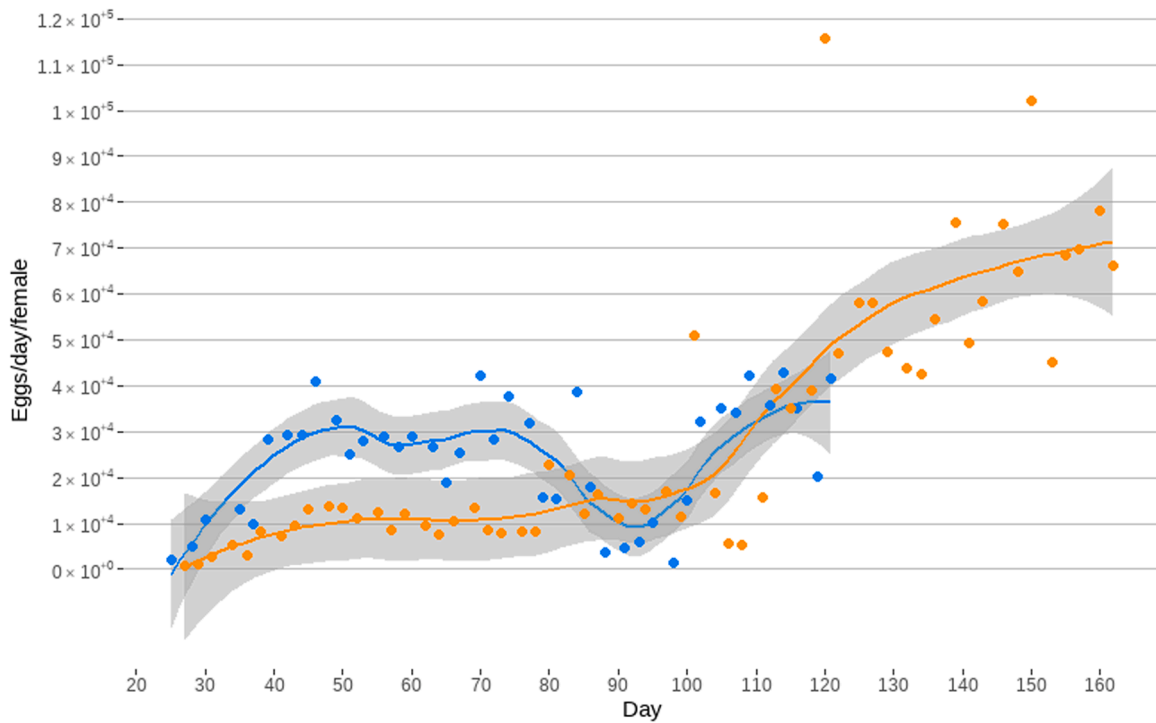


Fig. 1. Number of eggs shed per day and female for batch of *Anisakis pegreffii* (blue) and *Anisakis simplex sensu lato* (orange) cultured *in vitro*.

between days 5–7.

3.3. *A. pegreffii* L2 survival and exsheathment

*A. pegreffii* L2 showed a high survival and growth rate under all conditions tested, except for larvae in SSS (control) where no growth was observed, although the majority remained alive and active until the middle of the sixth week. Larvae in the highest osmolarities (700 and 800 mOsm) and in the mixture of SSS and DSM (1:1) had the highest survival rate throughout the experiment (Fig. 2). Significant differences in survival rates for the different conditions tested were observed

between the 6th and 10th week of the experiment. However, the higher survival rates (i.e., at 700 mOsm, 800 mOsm and the SSS + DSM mixture) did not show a significant difference between them at any time-point during the experiment (Table 1).

Detachment of the outer cuticle (L2) began at the end of the third week for larvae in 300, 400 and 600 mOsm and during the fourth week for larvae in SSS + DSM (1:1), 500, 700 and 800 mOsm. Interestingly, the control larvae in SSS did not shed the outer cuticle, except for a single specimen. The percentage of exsheathed larvae remained low under all conditions tested until the beginning of the sixth week. One week later (beginning of the seventh week), 100% of the remaining

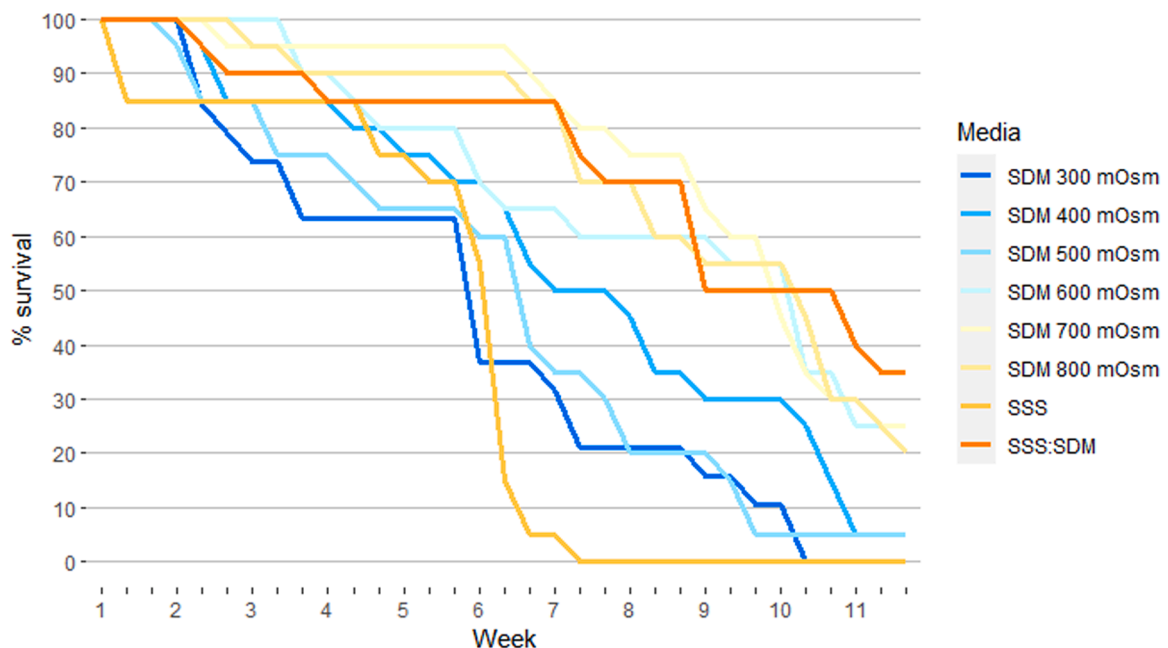


Fig. 2. Survival rate of *Anisakis pegreffii* larvae cultured *in vitro* under different osmolarities.

**Table 1**

Results of pairwise comparisons for survival and exsheathment rates of *Anisakis pegreffii* cultured in Schneider's *Drosophila* medium adjusted to different osmolarities (Fisher's exact test with Benjamini-Hochberg FDR correction). Only significant values ( $P < 0.05$ ) are shown.

	Survival <sup>a</sup>					Exsheathment <sup>b</sup>	
	W6	W7	W8	W9	W10	W6-D1	W6-D3
SSS-SSS:SDM		$3.79 \times 10^{-06}$	$3.12 \times 10^{-05}$	$3.05 \times 10^{-03}$	$4.07 \times 10^{-03}$		
SSS-SDM300							$3.58 \times 10^{-02}$
SSS-SDM400		$8.50 \times 10^{-03}$	$4.92 \times 10^{-03}$		$4.71 \times 10^{-02}$		$6.30 \times 10^{-03}$
SSS-SDM500							$7.49 \times 10^{-04}$
SSS-SDM600		$9.59 \times 10^{-04}$	$3.16 \times 10^{-04}$	$6.31 \times 10^{-04}$	$2.03 \times 10^{-03}$		$7.49 \times 10^{-04}$
SSS-SDM700		$3.79 \times 10^{-06}$	$2.16 \times 10^{-05}$	$3.61 \times 10^{-04}$	$5.83 \times 10^{-03}$	$4.76 \times 10^{-02}$	$3.08 \times 10^{-04}$
SSS-SDM800		$3.79 \times 10^{-06}$	$3.12 \times 10^{-05}$	$1.35 \times 10^{-03}$	$2.03 \times 10^{-03}$		$1.61 \times 10^{-04}$
SDM300-SSS:SDM	$2.86 \times 10^{-02}$	$4.24 \times 10^{-03}$	$9.27 \times 10^{-03}$		$3.51 \times 10^{-02}$		
SDM300-SDM400							
SDM300-SDM500							
SDM300-SDM600			$4.85 \times 10^{-02}$	$3.36 \times 10^{-02}$	$1.79 \times 10^{-02}$		
SDM300-SDM700	$3.84 \times 10^{-03}$	$4.24 \times 10^{-03}$	$4.92 \times 10^{-03}$	$1.71 \times 10^{-02}$			
SDM300-SDM800	$1.08 \times 10^{-02}$	$4.24 \times 10^{-03}$	$9.27 \times 10^{-03}$		$1.79 \times 10^{-02}$		
SDM400-SSS:SDM							
SDM400-SDM500							
SDM400-SDM600							
SDM400-SDM700							
SDM400-SDM800							
SDM500-SSS:SDM		$8.50 \times 10^{-03}$	$9.27 \times 10^{-03}$		$1.34 \times 10^{-02}$		$2.49 \times 10^{-02}$
SDM500-SDM600			$4.85 \times 10^{-02}$		$5.83 \times 10^{-03}$		
SDM500-SDM700		$8.50 \times 10^{-03}$	$4.92 \times 10^{-03}$	$3.81 \times 10^{-02}$	$2.34 \times 10^{-02}$		
SDM500-SDM800		$8.50 \times 10^{-03}$	$9.27 \times 10^{-03}$		$5.83 \times 10^{-03}$		
SDM600-SSS:SDM							$2.36 \times 10^{-02}$
SDM600-SDM700							
SDM600-SDM800							
SDM700-SSS:SDM							$1.57 \times 10^{-02}$
SDM700-SDM800							
SDM800-SSS:SDM							$5.29 \times 10^{-03}$

<sup>a</sup> Statistical differences in survival rate were assessed on counts corresponding to the first day of each week.

<sup>b</sup> Statistical differences in exsheathment rate were assessed for all counts during the weeks of the moulting process. D: day; SDM: Schneider's *Drosophila* medium; SSS: Sea Salt Solution; W: week. Note that the numbers ranging from 300 to 800 in the acronym of medium represent tested values of osmolarities.

larvae had shed the cuticle (Fig. 3) and these were considered third stage (L3) larvae. Significant differences in moulting rate were only observed at the midpoint of the experiment (week 6), which coincided with the peak of moulting. Differences were observed between the control (SSS) and the other conditions (except for the SSS + DSM mixture) and

between the SSS + DSM mixture and the higher osmolarities (500–800 mOsm) (Table 1).

L2 showed rapid and flicking movements before exsheathment, accumulated detritus on the outer cuticular sheath and few entangled L2 were usually observed. As the larvae grew larger and went through the

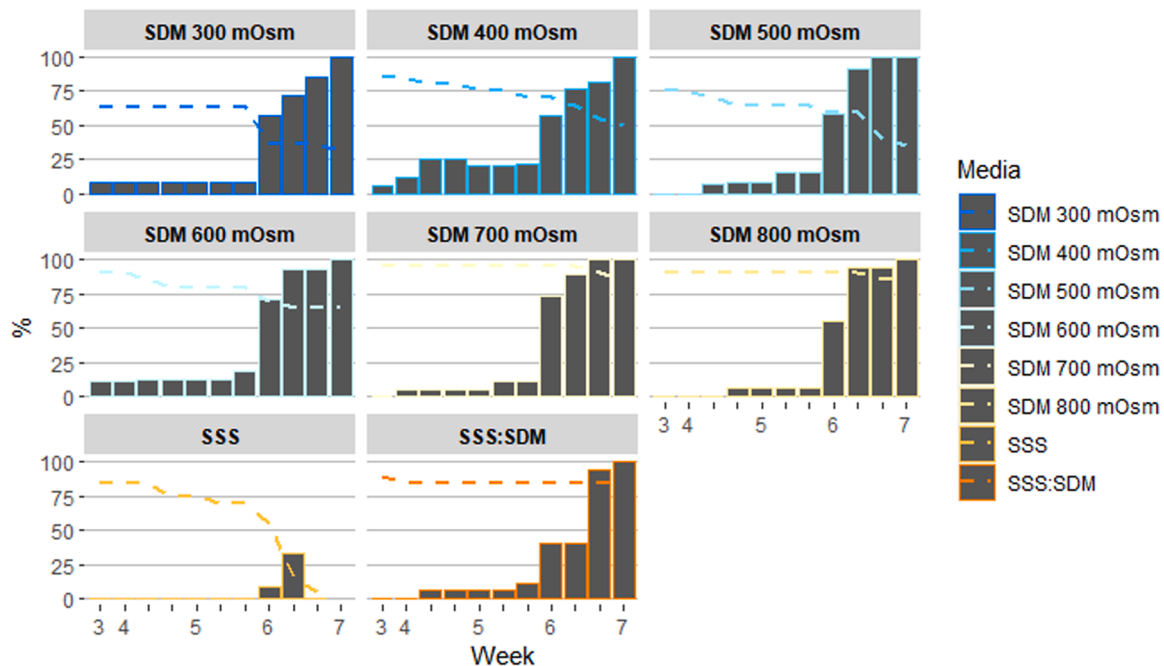


**Fig. 3.** Survival rate of *Anisakis pegreffii* larvae (dashed-line) and percentage of exsheathed larvae (bars) cultured *in vitro* under different osmolarities (independent graphs). The graph encompasses the period between the first exsheathment until 100% of larvae were exsheathed (x axis).

exsheathment process, their activity decreased, became more coiled (worm-like) and less detritus was observed attached to the L3 cuticle. During the exsheathment process, the larvae also showed constrictions due to cuticular rings (small remnants of the unshed cuticle), mostly in the anterior or posterior third of the body (Fig. 4a). Some L3 were able to overcome this, while some reached the “large L3 phenotype” with constrictions still visible. Most larvae managed to shed the cuticular ring (Fig. 4b). However, in some cases it was observed that the moulting process failed, and the constriction affected the development of the internal organs, leading to the death of the larva. Another moult of the developed L3 was observed after 3 months in culture, occasionally leaving cuticle at the tip of the tail.

### 3.4. Morphological characterization of *A. pegreffii* early developmental stages

#### 3.4.1. Morphology and morphometry

Morphometric measurements showed that the eggs increased in size during embryonic development while still maintaining a slightly ellipsoidal morphology (Table 2). The eggs and the recently hatched, double-sheathed L2 exhibited morphological characteristics consistent with those previously observed (Mladineo et al., 2023) (Fig. 5a-c).

The larvae in culture grew rapidly so that the body became tightly enveloped by the outer L2 cuticle, which previously only loosely encased the L2 at hatching. This led to the first exsheathment process of L2, marking the development of L3. L3 continued to grow in length and thicker, showing more developed internal organs. It is worth noting that two phenotypes could be observed during L3 growth, which we termed the “small L3 phenotype” (S3P) and “large L3 phenotype” (L3P), reflecting their significant difference in size. Table 2 summarises the morphometric data of each developmental stage. As the L3 grew, development continued at a slower pace, but typical L3 morphological features were observed: developed lips, boring tooth, a pharynx, a ventricle, a developed intestine (with peristaltic movements), a rectum and an excretory duct (Fig. 5d-g).

#### 3.4.2. Ultrastructure

**3.4.2.1. Embryogenesis of *A. pegreffii*.** The embryogenesis described herein is based on eggs collected on day 1 and day 6 of incubation. However, due to asynchronous development and hatching, the two time points could have contained eggs at different stages of development.

The eggshell consists of the outermost vitelline layer, a thick central chitin layer and an innermost lipid layer. The embryo is embedded in the thick electron-light substance enveloped by the plasma membrane, in which discharge of double-membrane vesicles (400 nm in radius) is sporadically observed (Fig. 6a). The unfertilised egg is acellular with numerous vacuoles with varying contents: electron dense, -light, granular, receding or absent (Fig. 6b). In an early blastula, a blastocoele is surrounded by six blastomeres that open into the lumen. On the opposite side, a cluster of five cells with a discrete rim of cytoplasm and a few small, electron-dense mitochondria is framed by two large cells (Fig. 6c). While one cell has a cytoplasm with elongated electron-dense



Fig. 4. A) Exsheathing larva of *Anisakis pegreffii* under contrast phase microscopy. The arrow points to the constriction caused by the cuticle of the second-stage larva (L2) and the arrowhead to the cuticle leftover. B) Recently shed striated L2 cuticle under light microscopy. Scale bars = 50  $\mu\text{m}$ .

Table 2

Morphometric measurements of early stages of *Anisakis pegreffii* cultured in Schneider's *Drosophila* medium (mean  $\pm$  standard deviation;  $\mu\text{m}$ ) recorded from each developmental stage.

	Eggs				
	N	Long axis	Short axis		
< 24 h	37	53.84 $\pm$ 4.03	48.18 $\pm$ 2.83		
Embryonated (5 d)	29	60.90 $\pm$ 4.95	56.03 $\pm$ 3.64		
	Larvae				
	N	Body <sup>a</sup>		Outer sheath	
		Length	Width	Length	Width
L2 - < 48 h	25	261.81 $\pm$ 29.73	22.06 $\pm$ 2.48	378.11 $\pm$ 20.69	28.99 $\pm$ 2.28
L2-3 weeks	16	338.42 $\pm$ 50.40	30.41 $\pm$ 7.79	399.87 $\pm$ 48.16	32.64 $\pm$ 6.90
L3-3 weeks	2	466.10 $\pm$ 44.60	50.50 $\pm$ 1.50	—	—
S3P - 17 weeks	1	463.94 $\pm$ 3.99	41.26 $\pm$ 0.36	—	—
L3P - 12 weeks	1	1684.70 $\pm$ 8.23	72.34 $\pm$ 6.23	—	—
L3P - 17 weeks	3	2273.56 $\pm$ 522.85	117.79 $\pm$ 4.41	—	—

S3P: small L3 phenotype; L3P: large L3 phenotype

<sup>a</sup> Body measurements of third-stage larvae (L3) were taken per triplicate to reduce the error derived from the use of the manual measuring tool applied for length (sinusoidal shape) and to provide the average of different body widths (proximal, middle and distal part). Width of second-stage larvae (L2) was taken at the level of mid pharynx.

mitochondria, vesicles and multivesicular bodies, the other has a network of convoluted tubular cisternae and sparse perilemmal vesicles (Fig. 6d). The early gastrulation stage shows somatic cells of the putative ectoderm with a large oval nucleus at the periphery, numerous ribosomes, relatively small mitochondria and accumulated glycogen (Fig. 6e). Large empty vacuoles or vacuoles with different electron densities, sometimes fusing together, were common in these cells. The presumptive germline cell is located in the middle of the gastrula and has a large and irregular nucleus (Fig. 6f). In the later gastrula, the number and size of cells increases, as does the abundance of cytoplasmic granules and vesicles, and the number of larger mitochondria (Fig. 6g). A single conspicuous cell with a network of developing intracytoplasmic ducts connecting to form a lumen is noted, surrounded by cells connected by numerous tight junctions (Fig. 6h).

**3.4.2.2. Early ontogenesis of *A. pegreffii*.** The ontogeny described here is based on L2 between 0 and 48 h of age after hatching. In most cases, L2 were observed with the inner cuticle 3 tightly attached to the epidermis and with a loose, enveloping cuticle 2 in the process of shedding.

At the level of the posterior end of the buccal cavity, the excretory channel attaches to the epidermal cell and runs between two anterior nerve cords (Fig. 7a). The pharynx consists of six firmly connected epithelial cells with a large spherical nucleus rich in ribosomes, vesicles and few mitochondria. The lumen is closed, Y-shaped and lined with proteinaceous calix (Fig. 7b-c). A nerve ring of neurons and neurite bundles consisting of microtubules and neurotransmitter granules surrounds the pharynx (Fig. 7d-f).

A putative EGC is already noticeable in L2. The anterior part of its excretory channel passes at the level of the pharynx and shows secretion of what looks like EVs (Fig. 8a-c). The nucleus of the EGC is larger, irregular in shape, almost lobate and with a less condensed chromatin than in somatic cells (Fig. 8d-f). The cytoplasm is rich in ribosomes, few mitochondria and granules and vesicles of varying size and content. A fluid-filled excretory lumen forms a wide receptacle in the central part of the cell, extending posteriorly above the nucleus (Fig. 8g-i).

Occasionally, various structures are secreted between the cuticle

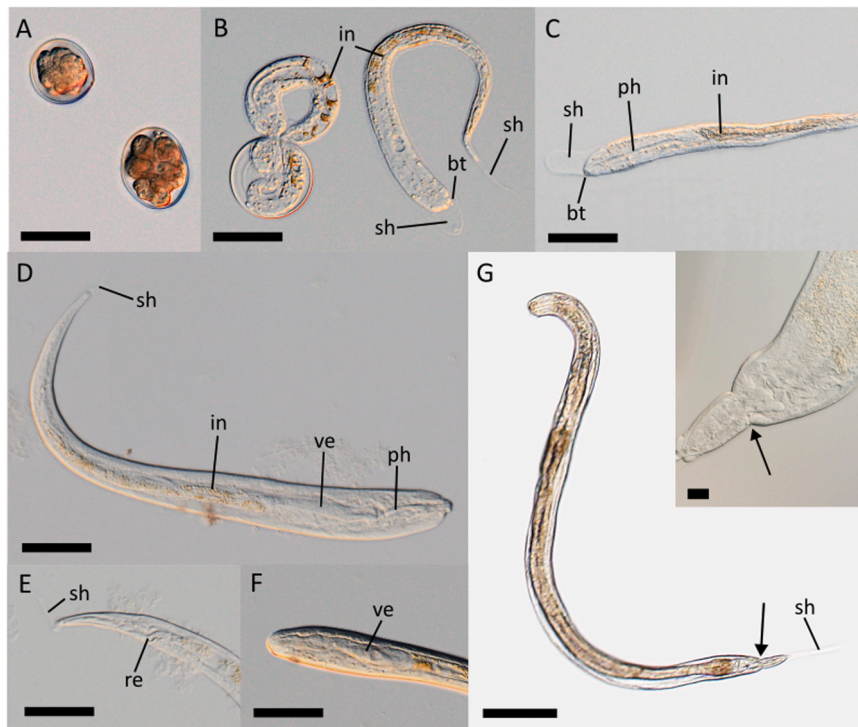


**Fig. 5.** Eggs and larvae of *Anisakis pegreffii* under contrast phase microscopy. A) Eggs at early stages of embryonic development; note the triple-layer, smooth eggshell. B) Larva hatching and recently hatched second-stage larva (L2). C) Double-ensheathed L2. D) Fully developed larva before exsheathment. E) Posterior end of a fully developed larva before exsheathment. F) Anterior part of a fully developed larva before exsheathment. G) Exsheathed third-stage larva (L3) (large L3 phenotype). The inset is the detail of the posterior end, showing the constriction caused by the leftover of the L2 cuticle (arrow). bt: boring tooth; ph: pharynx; in: intestine; sh: outer sheet; re: rectum; ve: ventricle. Scale bars: 50 µm a-f; 200 µm g; 20 µm inset in g.

attached to the L2 epidermis (i.e., cuticle 3) and the exsheathed, loose cuticle in the process of shedding (cuticle 2) (Fig. 9a). These include larger microvesicles (Fig. 9b), granules with different contents (Fig. 9c-d), cell-free mitochondria (Figs. 9a, 9c) and EVs (Fig. 9e). Neurotransmitter release by peripheral neurons to myocytes is also observed in the larval epidermis (Fig. 9f).

Six epithelial cells form the lumen of the putative intestinal tract, which is filled with electron-lucent material. In its part proximal to the pharynx, the intestine is flanked by the posterior part of the EGC, recognisable by the excretory channel, numerous ribosomes and the rough endoplasmic reticulum (Fig. 10a). Further aborally, the intestine extends in the lumen and is surrounded by a second layer of densely packed epithelial cells interspersed with neurite bundles and myocytes that form the epidermis (Fig. 10b-c). At the largest diameter of the gut, the lumen consists of only a single epithelial cell (Fig. 10d). In the most caudal part, after the anal opening, the body consists of bundles of neurites, a few epithelial cells and epidermal myocytes (Fig. 10f-h).

### 3.5. Karyotype

The protocol applied for preparing chromosome spreads allowed us to obtain *A. pegreffii* chromosomes at different cell stages (Fig. 11a-c). The mitotic metaphase nuclei (Fig. 11c) were detected in 3 specimens (two females and one male), although not in large numbers. Thirty mitotic metaphase cells were counted, which had variable numbers of 15–20, potentially holocentric, chromosomes. The most frequently recorded number was 18 (43.33%; N = 13), suggesting a diploid karyotype formula of  $2n = 18$ . The remaining cells showed counts of 20 (23.33%; N = 7), 19 (13.33%; N = 4), 17 (10% each; N = 3), 16 (6.67%; N = 2) and 15 (3.33%; N = 1) chromosomes.

The positive telomeric signal (TTAGGC)<sub>n</sub> in *A. pegreffii* showed consistently variable intensity between chromosomes and between the ends of the same chromosome. A strong interstitial block of telomeric

repeats was observed in some chromosomes (Fig. 11d).

## 4. Discussion

### 4.1. Fecundity

Although expected, this study is the first proof of concept that the culture conditions developed for *A. pegreffii* also support well the development and reproduction of *A. simplex*. Furthermore, it must be taken into account that the *A. simplex* batch we used in the experiment also contained specimens of *A. pegreffii* to a small extent, as the batch originated from a sympatric area of *Anisakis* spp. (i.e., from the North Atlantic).

Several studies have reported on egg production of female anisakids, but they have mainly relied on counting eggs from dissected uteri (McClelland, 1980; Smith, 1988; Marcogliese, 1997; Iglesias et al., 2001). Fecundity data obtained from naturally deposited eggs of nematodes in culture are scarce and only from *A. simplex* (Iglesias et al., 2001; Ugland et al., 2004). Iglesias et al. (2001) reported only two females that laid a maximum of 5672 and 16,790 eggs per day, which is far from our maximum, 115,694.45 eggs/day/female. However, these authors used a different culture medium based on RPMI-1640 with 20% (v/v) heat-inactivated foetal bovine serum and 1% pepsin, which was inconsistent in achieving oviposition. Ugland et al. (2004) registered oviposition in *A. simplex* females from minke whale cultured in sterile water containing 0.9% NaCl (pH=5–6). These females laid a higher number of eggs than in this study, but 98% of them were laid in the first six days. The saline water cannot sustain nematodes under their physiological conditions, therefore the discharged eggs were probably released from stressed and dying animals in a nutrient-depleted medium.

These are the first data on the fecundity of *A. pegreffii* (i.e., 24,370.96 eggs/day/female average production), which is almost 19% less than

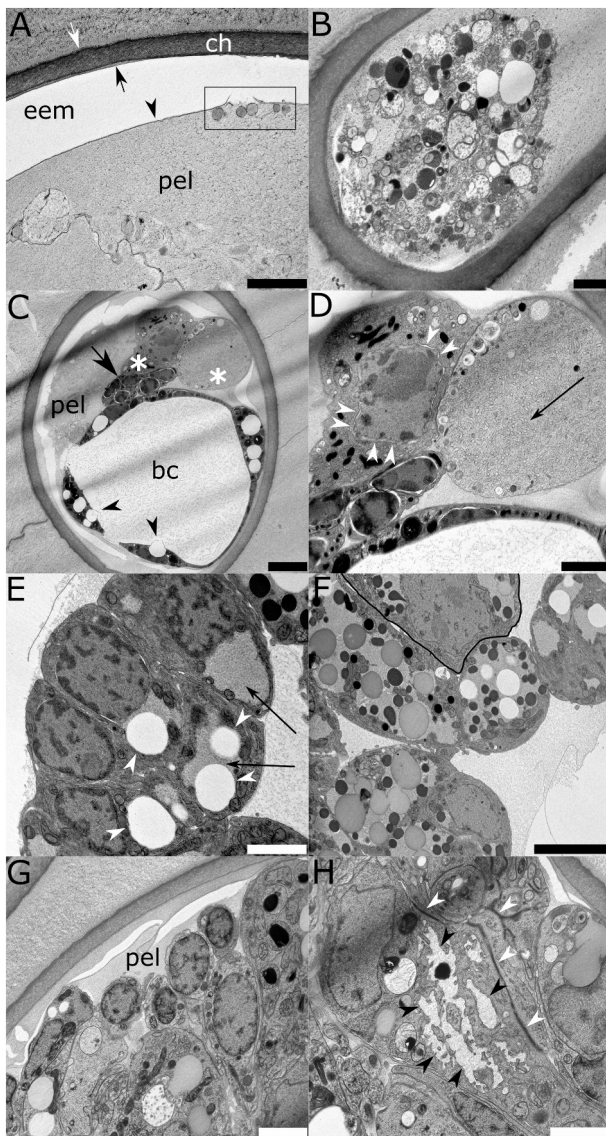


**Fig. 6.** Representative transmission electron micrographs of *Anisakis pegreffii* embryogenesis within the egg: A) Trilaminar eggshell consisting of the vitelline layer (white arrow), chitinous layer (ch) and lipid layer (black arrow). Below the eggshell, fluid-filled extra-embryonic matrix (eem) envelops the amorphous peri-embryonic layer (pel) that envelops the embryo (not shown). Peri-embryonic layer is bordered by a thin double-layered permeability barrier (black arrowhead). Black rectangular demarcates the site of double-membrane vesicles secreted into the extra-embryonic layer; B) Acellular unfertilised eggs with numerous granules and vesicles; C) Early blastula with blastomeres surrounding the blastocoel (bc), a cluster of small cells (black arrow), and two larger cells (white asterisk) enveloped in peri-embryonic layer (pel). Note blastomeres' vesicles discharging in the blastocoel (black arrowhead); D) Higher magnification of two larger cells in the early blastula. Note the irregular shape of the large nucleus with distinct nuclear membranes in the left cell (white arrowheads) and the abundant tubular network reminiscent of cisternae in the right cell (black arrow); E) Putative ectodermal cells in the gastrula with an apical rounded nucleus and fluid-filled vesicles (white arrowhead) and glycogen accumulations (black arrow) interspersed within the cytoplasm; F) Putative germline cell with a large and irregular nucleus (demarcated by a black line); G) Somatic cells in the late gastrula rich in granules and vesicles, enveloped by periembryonic layer (pel); and H) Putative excretory gland cell, whose cytoplasm is interspersed by branching channels (black arrowhead), reminiscent of the lumen of excretory channel. Note strong tight junctions between somatic cells (white arrowhead). Scale bars: 2  $\mu$ m a, b, d, e, g and h; 5  $\mu$ m c and f.

the average fecundity of *A. simplex*. However, this interpretation should be taken with caution, as the two experiments lasted for different lengths of time and we observed increased production in *A. simplex* batch in the last days (Fig. 1).

Fertility (or hatching rate) was not assessed in this study, although there are previous reports for both *A. simplex* and *A. pegreffii* at different temperatures, from 3 °C to 25–27 °C (88–95% and 1–47% mean hatching rates, respectively; Gomes et al., 2023), as well as for other related nematodes (*C. multipapillatum* in Valles-Vega et al., 2017 and *Hysterothylacium aduncum* in Adroher et al., 2004).

#### 4.2. Culture medium characteristics

Schnider's *Drosophila* medium supplemented with 10% CS, has been shown to be effective in maintaining and developing the early stages of *A. pegreffii* (i.e., from L2 to L3), based on its previous use in the culture of the late developmental stages of *A. pegreffii* (from L3 to adults) (Mladineo et al., 2023). Although the medium was originally intended for the culture of insect cell lines, some studies suggest that it is more suitable for the development of nematodes than media for vertebrate cell lines (Adroher et al., 2004; Mladineo et al., 2023). Given insects and nematodes evolutionary relatedness, particularly their shared experience of ecdysis, a key developmental process (Giribet and Edgecombe, 2017), the medium is expected to support the development of early nematode stages in which multiple ecdyses occur. The low concentration of CS chosen (10%) allowed for balanced L2 growth that correlated with the moulting process, in contrast to the high concentration tested previously (50%), which stimulated rapid growth but was not associated with timely moulting (Mladineo et al., 2023). CS as opposed to foetal bovine serum (most commonly used as a nutrient source) proved to be suitable for both late and early developmental stages of *A. pegreffii* (Mladineo et al., 2023). Moreover, CS has been successfully used for *in vitro* culture of marine trematodes (Fredensborg and Poulin, 2005; Lloyd and Poulin, 2011), suggesting that this serum may be more suitable for the culture of marine helminths than for terrestrial ones.

Some marine invertebrates are osmoconformers that maintain their internal environment isotonic to their external seawater environment. Although there are few data specifically for marine helminths, it seems that their culture success is influenced by the osmolarity of the medium (de Meester et al., 2011; Xie and Zhang, 2022; Podbielski et al., 2022). Considering that the osmolarity of SDM ranges from 320 to 360 mOsm according to the manufacturer's certificate of analysis, we tested different osmolarities on the early developmental stages of *Anisakis* and found that the best survival rates were obtained with the highest (700 and 800 mOsm) and with SSS (1200 mOsm) + SDM (1:1). Marine crustaceans, which serve as the first intermediate hosts for anisakids, are also osmoconformers, therefore high osmolarities that mimic biological conditions in krill and other crustaceans allow higher survival rates of early larvae of *A. pegreffii*. Although the use of SSS + SDM is more economical compared to SDM for massive larval rearing, it is limited by the delay in L2 exsheathment compared to the one observed in L2 in high osmolarity SDM, which hampers its application.

#### 4.3. Early development of *A. pegreffii*

To our knowledge, this is the first time that the development of *Anisakis* spp. from L2 to L3 has been achieved *in vitro*. In fact, only for one related taxon, *Contraecaecum multipapillatum*, has an attempt been made to develop and characterise *in vitro* hatched larvae (Valles-Vega et al., 2017). However, the experiment was short-termed (25 days) and only  $\approx$  2% of the larvae exsheathed. Hatched *C. multipapillatum* and larvae of other anisakids show flicking movements and attachment of detritus before exsheathing, similar to *A. pegreffii* L2 described here (Thomas, 1937; Huizinga, 1966; Davey, 1969; McClelland and Ronald, 1974; Højgaard, 1998; Adroher et al., 2004). After exsheathment, *A. pegreffii* shows more serpentine, worm-like movements and adheres

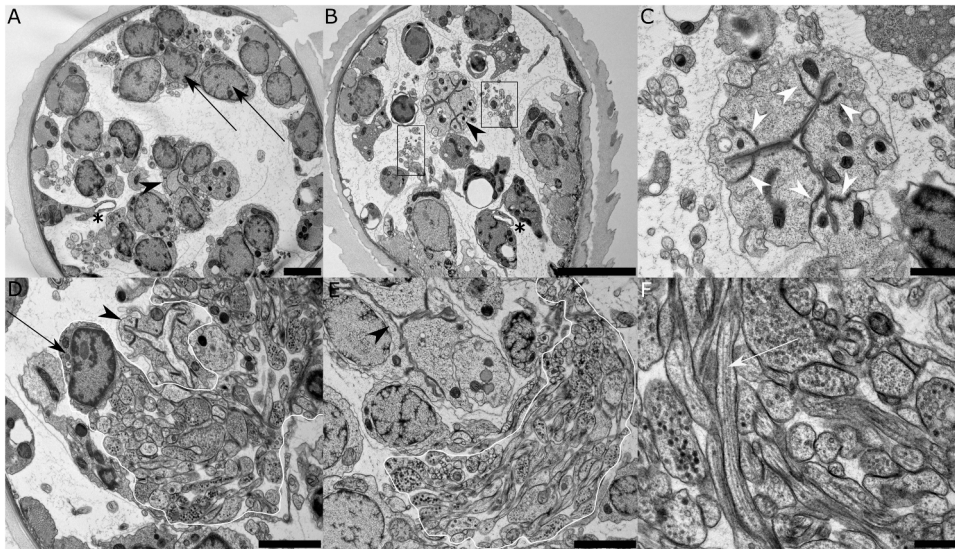


**Fig. 7.** Representative transmission electron micrographs of *Anisakis pegreffii* L2 cross-section at the pharynx level: A) Posterior part of the buccal cavity (black arrowhead) proximal to the excretory channel (black asterisk) and neurons filled with neurotransmitters' granules (black arrows); B) Y-shaped pharynx lumen (black arrowhead) surrounded by two bundles of neurites (black rectangles) and the excretory channel (black asterisk); C) Higher magnification of six epithelial cells forming the pharynx. Note tight junctions between cells (white arrowheads); D) and E) Neurons (black arrow) and neurites (demarcated by a white line) circumventing the pharynx (black arrowhead); and F) Higher magnification of bundles of neurites consisting of neurotubules (white arrow) and granules of neurotransmitters. Scale bars: 500 nm f; 1  $\mu$ m c; 2  $\mu$ m a, d, e; 5  $\mu$ m b.

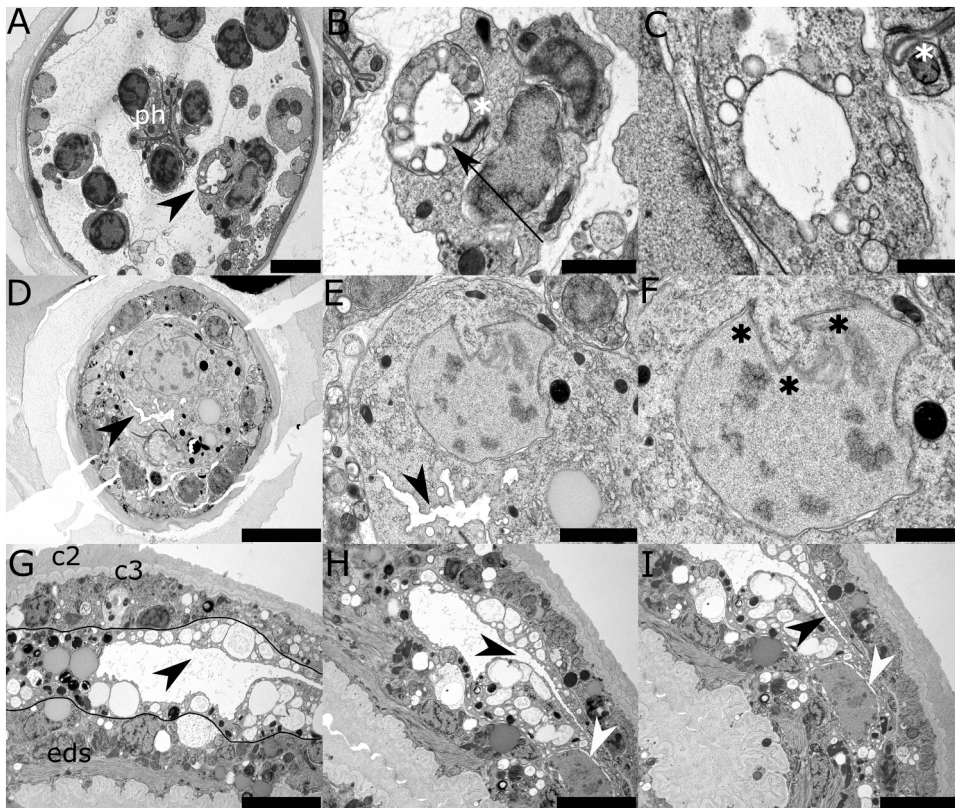


**Fig. 8.** Representative transmission electron micrographs of *Anisakis pegreffii* L2 putative excretory gland cell (EGC): A) Cross section of L2 at the pharynx (ph) level, sided by anterior part of the excretory channel (black arrowhead); B) Higher magnification of the excretory channel filled with fluid and secreted extracellular vesicle (black arrow). Note the apparent junction of the channel to the adjacent somatic cell (white asterisk) that in consequent section in C) disappears, suggesting a transient point of attachment to the epidermis; D) Cross section through body of the putative EGC at the level of excretory channel lumen (black arrowhead); E) Higher magnifications showing irregular lumen of the excretory channel with smaller connecting canaliculi (black arrowhead); F) Large EGC nucleus, with a lobed and irregular appearance (black asterisks); and G-I) Longitudinal consecutive sections of L2 at the level of EGC (demarcated by a black line), showing anteriorly a receptacle formed by excretory channel (black arrowheads) that posteriorly diminishes in the diameter, directed dorsally to the cell nucleus (white arrowheads). Scale bars: 500 nm c; 1  $\mu$ m b, f; 2  $\mu$ m a, e; and 5  $\mu$ m d, g-i.

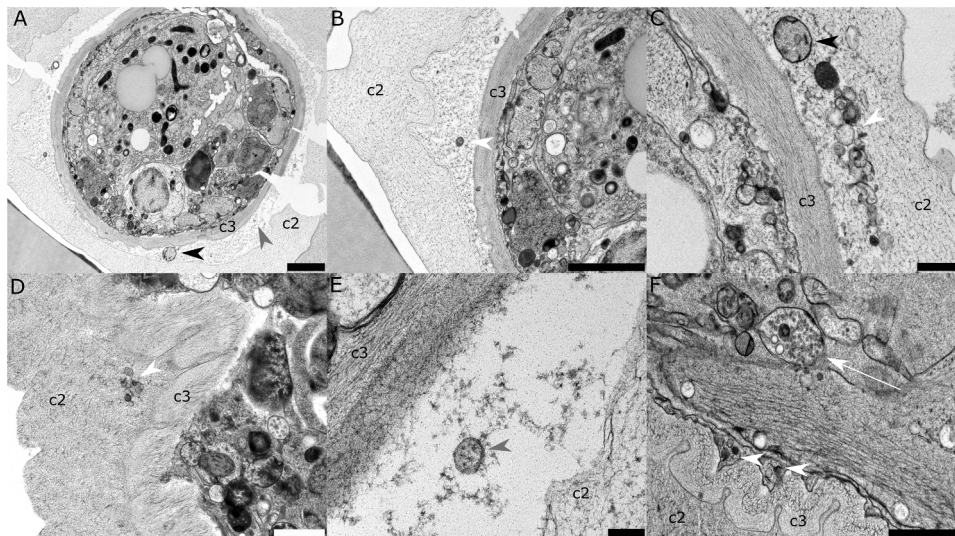


**Fig. 9.** Representative transmission electron micrographs of *Anisakis pegreffii* L2 secretion: A) Cell-free mitochondria (black arrowhead) and extracellular vesicles (grey arrowhead) shed between larval cuticle 3 (c3) and lose cuticle 2 (c2); B) Large microvesicle (white arrowhead); C) and D) Accumulation of granules with different content (white arrowhead) and a cell-free mitochondria within cuticle 2 that is still tightly attached to cuticle 3 at the epidermal surface; E) Extracellular vesicle (grey arrowhead) with double membrane secreted between cuticle 3 and 2; and F) Neuron cell releasing neurotransmitters at the myocytes synapses in the epidermis (white arrow). Note accumulation of granules (white arrowheads) between epidermis and cuticle 3. Scale bars: 200 nm e; 500 nm c; 1  $\mu$ m d, f; 2  $\mu$ m a, b.

less to substrates. We suggest that this is due to better developed somatic myocytes, the properties/composition of the newly obtained cuticle and/or the development of sensory structures that help to avoid detritus. Valles-Vega et al. (2017) observed exsheathment over 25 days only in *C. multipapillatum* larvae maintained at 24 °C, that started on the 14th day of the experiment. In contrast, *A. pegreffii* started to exsheath on 3rd week of the experiment, at a lower temperature than *C. multipapillatum* (i.e., 19 °C). This is consistent with previous reports where higher temperatures were associated with faster development of both nematode eggs and larvae, but with lower larval survival (Bratney and Clarck, 1992; Measures, 1996; Højgaard, 1998; Valles-Vega et al., 2017; Gomes et al., 2023). In addition, the inability to completely shed a piece of cuticle during exsheathment led to larval strangulation in some cases. In *C. multipapillatum*, moulting occurs in the gut of the copepod (Huizinga, 1967), suggesting that host digestive enzymes are involved in this process, as is known for several proteases involved in nematode moulting (reviewed in Page et al., 2014). *A. pegreffii* moults to L3 in the crustacean haemocoel (Smith, 1983), but since reaching the haemocoel implies previous intestinal or hepatopancreatic migration, digestive enzymes may also be involved in the natural exsheathment process.

In agreement with the observations of Valles-Vega et al. (2017) in *C. multipapillatum*, freshly hatched larvae of *A. pegreffii* already show the boring tooth, pharynx and developing intestine being ensheathed in the striated cuticle of the L2 stage. The development of the organs begins during postembryonic growth, and after exsheathment all the morphological characteristics of the L3 stage are visible, except for the mucron, which becomes present in older L3 stages. Despite the long duration of the experiment (17 weeks for the last larvae in culture), the L3 did not reach the size of *A. pegreffii* L3 that naturally infects the fish. In this study, the mean length of L3P was 2.27 mm, far below the mean length of L3 from natural fish infections (e.g., 16.9 mm, Roca-Geronès et al., 2020). Although we detected peristalsis of the intestinal tract, similar to *C. papillatum*, there was no evidence of active feeding, which is expected for L3 surviving in fish in an inactive state of paratenesis (Trumbić et al., 2021).

Finally, it is noteworthy that the older L3 stage differentiates into a large and a small phenotype under the same culture conditions. This is comparable to the appearance of giant *Cenorhabditis elegans* after induction of oocytes fusion by a laser microbeam; the newly formed oocyte continued its normal cleavage pattern after fusion, suggesting

regulation by the uncleaved oocyte (Irlle and Schierenberg, 2002). Although we cannot link our observation to the manipulation of *C. elegans* oocytes, it remains to be clarified whether this process is a natural part of *A. pegreffii* ontogeny or whether it is conditioned by an artificial environment.

In summary, *A. pegreffii* moults once in the egg, hatches as L2, subsequently shedding the ensheathed L2 cuticle and becomes L3, with corresponding L3 traits, except for the mucron, which develops in the older L3 stage. Moreover, an additional moult was observed in the older L3 stage, but this was not accompanied by a physiological or morphological shift to the L4 stage. Although an additional moult caused only by nematode growth cannot be ruled out, it is unexpected as the cuticle of nematodes is collagen-based and therefore allows growth during intermediate moulting periods (Lažetić and Fay, 2017). Alternatively, supernumerary moults could occur, as described in *C. elegans*, due to mutations in heterochronic genes (Ambros and Horvitz, 1984; Ambros, 1989).

#### 4.4. Ultrastructure

Milestone studies on the embryonic and postembryonic development of nematodes are based on two model taxa: *Parascaris equorum* (syn *Ascaris megalcephala*) and *C. elegans*. Although they share the same pattern of asymmetric divisions giving rise to somatic founder cells and germline cells, in *P. equorum* a rare phenomenon of chromatin loss due to breakage and degradation of chromatin during early blastomere cleavages results in silencing of somatic genes (Schierenberg and Sommer, 2014). In *C. elegans*, however, each new cell lineage expresses a specific cell cycle rhythm and a fixed cleavage and differentiation programme, including apoptosis, as a distinct cell fate (Schierenberg and Sommer, 2014). In the phylum Nematoda, evolution contributed to the development of substantially divergent cleavage patterns, spatial arrangements and differentiation of cells, but these features were not followed by corresponding phenotypic changes (Schulze and Schierenberg, 2011). Although taxa share the same characteristic developmental steps, these are achieved through different cell behaviour, so that even within the same species, different scenarios of nematode embryogenesis occur.

Although describing the embryogenesis of *A. pegreffii* is beyond our scope, we have observed snippets of the process that are worth

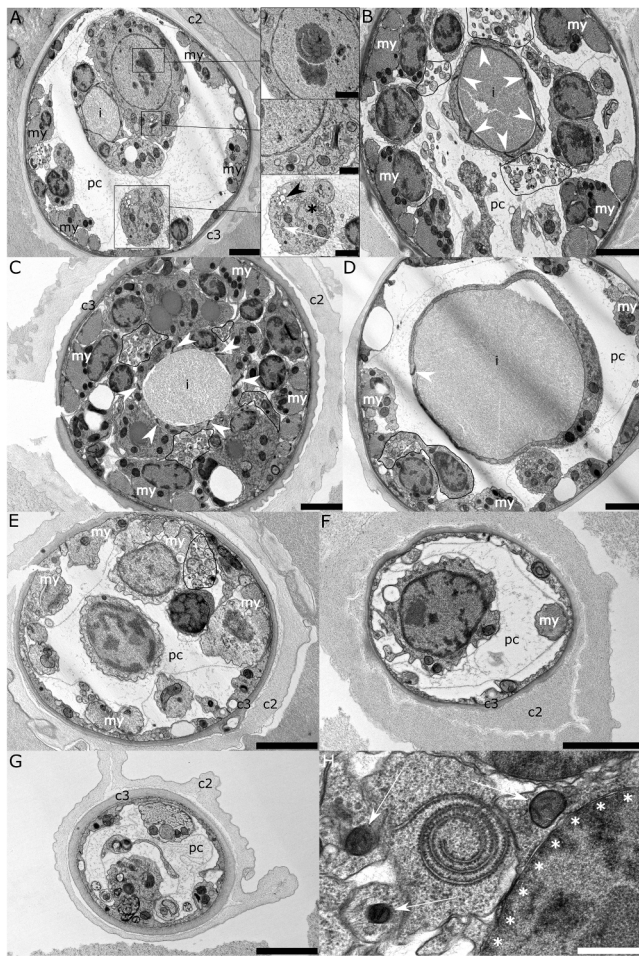


**Fig. 10.** Representative transmission electron micrographs of *Anisakis pegreffii* L2 cross secretions from the intestinal level toward caudal end: A) Putative upper part of the intestine filled with electron-light material. Highlighted in three black rectangles are higher-magnification insets detailing the epithelial cell nucleolus (top inset), Golgi apparatus proximal to nuclear membrane (central inset), and distal part of the excretory gland cell (bottom inset). The latter encompasses the posterior distal part of the excretory channel (black arrowhead), tubular rough endoplasmic reticulum (white arrow) and Golgi apparatus (black asterisk); B) Intestinal lumen made by six epithelial cells connected by tight junctions (white arrowheads), proximal to three bundles of neurites (demarcated by a black line); C) Intestinal lumen surrounded by two layers of epithelial cells. Bundles of neurites (demarcated by a black line) are interspersed between the second layer of epithelial cells. Note the first layer of six epithelial cells that form the lumen (white arrowheads); D) More distal intestinal segment formed by a single epithelial cell (tight junction marked by white arrowhead). Note a neuron and bundles of neurites (demarcated by a black line); E) – G) Caudal segments after the anal opening; and H) A detail of cylindrical rough endoplasmic reticulum proximal to the nuclear envelope (white asterisks) and small mitochondria (white arrows). i: intestine; my: myocytes in epidermis; pc: pseudocoelom; c2: larval cuticle 2; c3: larval cuticle 3. Scale bars: 500 nm central inset, 1 µm top and bottom inset; 2 µm a-g.

discussing. In the early blastula, for example, the number of blastomeres forming the blastocoele is six, which corresponds to the number of epithelial-like cells forming the pharynx and the intestinal tube of L2 in early postembryonic development. Six blastomeres are supplied with large vacuoles that discharge the liquid content into the newly formed blastocoele cavity. This is consistent with the recognised pattern of blastocoele formation based on successive divisions along the surface plane of the embryo that drive the blastomeres to form a spherical sheet surrounding the cavity (Wolpert et al., 2015). Biophysical approaches in *C. elegans* suggest that the cavity is formed by the growth and coarsening

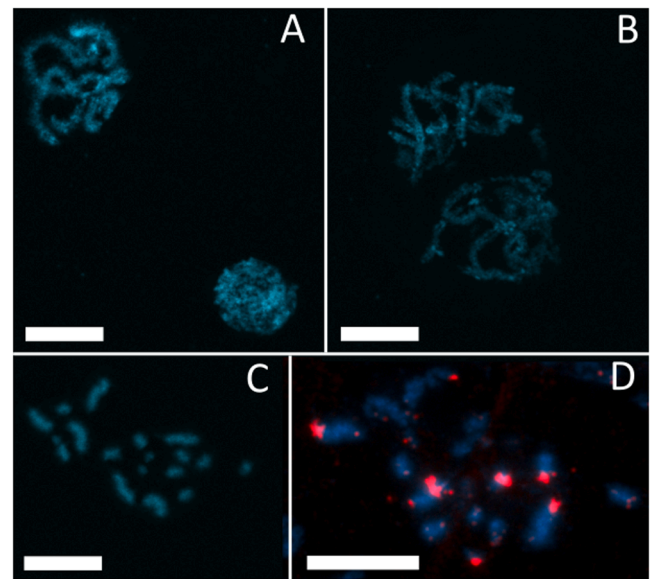


**Fig. 11.** *Anisakis pegreffii* chromosomes at different stages of the cell cycle stained with DAPI (blue) and after fluorescence *in situ* hybridization (FISH) with biotin-labeled telomeric probe (red). A) Cells in interphase (down) and pachytene (up) stages; B) pachytene stage; C) mitotic metaphase. D) Cell in a mitotic metaphase with chromosomes (in blue) showing a positive signal of nematode telomeric sequences (in red). Scale bars = 10 µm.

of myriad of micrometric lumens connected by the intercellular space between blastomeres (Le Verge-Serandour and Turlier, 2021), but we have not been able to observe early-stage embryos to confirm this.

A cell strikingly larger than other somatic cells in *A. pegreffii* L2 was observed 72 h after hatching using confocal microscopy (Mladineo et al., 2023). Based on its size and localisation, the authors speculated that the cell will develop into the EGC, but could not provide further evidence due to the lack of specific cell markers. The EGC is one of the most important cells for the survival of parasitic nematodes. It facilitates enzymatic degradation of host tissues, larval penetration and migration, feeding, antigenic interaction with the host immune system, modulation of T-helper and innate immunity axes, and antimicrobial activity within the host gastrointestinal system *via* excretion and secretion of bioactive compounds released directly in the secretome or packaged in EVs (Baeza et al., 2004; Cotton et al., 2012; Bahlool et al., 2013; McSorley et al., 2013; Fæste et al., 2014; Harnett, 2014; Lee et al., 2017). Here, we described an elongated cell in 48-h-old L2 rich in granules and vesicles, with a large and irregularly shaped nucleus and a channel intersecting the cytoplasm longitudinally and broadening into a central receptacle, reminiscent of EGC. The anterior L2 cross-sections at the pharyngeal level allowed observation of the excretory channel leaving EGC on its way out through the excretory pore. EVs and fluid secreted in its lumen indicate that already early L2 stage interacts with its environment. The role of the EGC in nematode ecdysis (Davey and Kan, 1968) and the observation that the first moult already occurs in the egg support the assumption that the EGC differentiates during embryonic development and is already functional before larval hatching. Interestingly, we observed an accumulation of EVs, granules and cell-free mitochondria in the space between the loose L2 cuticle and the tight L3 cuticle on the epidermal surface. While EVs, which were also observed in the excretory channel, could have been expelled through the excretory pore and smaller granules were observed passing through the L3 cuticle, cell-free mitochondria are a rare observation. Indeed, mitochondria are expelled from the cell during developmental processes in some cells, either freely or membrane-enveloped, as both proinflammatory and anti-inflammatory mediators, or in the case of their damage in post-mitotic cells, during a “garbage clearance” (Lyamzaev et al., 2022).

Several models have described this process in human and fish cell lines, as well as in squirrel retinal cones, while in *C. elegans* adult neurons release large protrusions containing mitochondria and protein aggregates in the form of “exophers” during neurotoxic stress (Melentijevic et al., 2017). To our knowledge, this is the first observation of cell-free mitochondria during the ontogeny of a parasitic nematode. Since mitochondria possess properties typical of ancestral bacteria, and their components are recognised as damage-associated molecular patterns (DAMPs) capable of activating pattern recognition receptors (PRRs), their immunomodulatory properties have been demonstrated (Zhang et al., 2010; Krysko et al., 2011; Sarhan et al., 2018). It remains to be proven whether cell-free L2 mitochondria are discharged with the intention of interacting with haemocytes of the first intermediate host.

#### 4.5. Karyotype

Cytogenetic studies have an important role in taxonomy and can help classify sibling species that are morphologically indistinguishable. This is particularly important in parasitic helminths, where correct identification is essential for accurate epidemiological management and effective treatment (Nielsen et al., 2014; Tanveer et al., 2015). Despite the fact that anisakiosis is one of the most important fish-borne parasitic diseases, there are no cytological data for members of the genus *Anisakis*. This could be due to the unavailability of live adults needed for the protocol, which relies mainly on gonadal tissue with its high rate of proliferating cells. To our knowledge, within anisakids, chromosome number data have only been reported for three *Contracaecum* species, namely *C. clavatum*, *C. incurvum* and *C. spiculigerum* (Goodrich, 1916; Walton, 1924; Walton, 1940). In contrast, the closely related family Ascarididae is well studied (Tanveer et al., 2015).

Here we report for the first time a protocol for obtaining *A. pegreffii* chromosome spreads, and provide the first chromosome count. Although it is advisable to increase the number of specimens to obtain a higher number of metaphasic cells, which was limiting herein due to the preservation of live adults to study their fecundity, our preliminary result suggests that *A. pegreffii* has a diploid number of  $2n = 18$ , possibly holocentric chromosomes (a more detailed technique would be necessary to confirm holocentricity). It is known that most nematodes have holocentric chromosomes (Carlton et al., 2022), and worms with sexual reproduction tend to be diploid (Benazzi, 1982). Our observation of cells with lower or higher chromosome numbers in some cases could be explained as an artefact of spreading, inherent to the procedure. Low numbers may result from the loss of some chromosomes in the metaphases, especially the smaller ones. Conversely, higher chromosome numbers may be the result of chromatids splitting into two parts (Orosová et al., 2021).

We have validated the proof of concept of nematode telomeric probe (TTAGGC)<sub>n</sub> in *A. pegreffii*, demonstrating the presence of a conserved repetitive telomeric sequence also in a marine nematode. The telomeric sequence of nematodes was discovered in *Ascaris suum* (Müller et al., 1991) and has only been studied in two subgroups of nematodes, Rhabditida and Ascaridida (Traut et al., 2007). However, we observed variability in signal intensity in the telomeric endings of *A. pegreffii* chromosomes, which may be due to hypervariability in the length of telomeric repeats (Starling et al., 1990; Rocco et al., 2001). This is not unusual, as in some cases even a complete absence of telomeric signal can be detected, which is due to low copy number of DNA repeats and/or non-clustered organisation of these tandem repeats. To better visualise telomeric signals of *A. pegreffii*, tiramide signal amplification FISH (TSA-FISH) could be used as a suitable approach (Cabral-de-Mello and Marec, 2021). Finally, the presence of interstitial telomeric sequences (tandem repeats of telomeric sequence at intrachromosomal positions) in *A. pegreffii* suggests structural rearrangements of chromosomes during nematode evolution (Lin and Yan, 2008).

The karyological information is not only a useful taxonomic tool but, complemented by PacBio long read sequencing technology in

combination with conventional short read sequencing, also enables whole-chromosome assemblies of genomes. This is crucial to fill gaps created by repetitive DNA and to achieve greater accuracy in estimating the genome size of helminths. This is important for translational studies focused on the treatment of neglected helminthiasis (Carlton et al., 2022; Doyle, 2022).

#### CRediT authorship contribution statement

**Samantha Moratal:** Writing – original draft, Visualization, Methodology, Investigation, Formal analysis, Data curation. **Magda Zrzavá:** Writing – review & editing, Resources, Methodology, Investigation. **Jerko Hrabar:** Writing – review & editing, Resources, Methodology, Investigation, Formal analysis. **Jordi López-Ramon:** Writing – review & editing, Formal analysis. **Ivona Mladineo:** Writing – review & editing, Writing – original draft, Visualization, Supervision, Resources, Methodology, Investigation, Conceptualization.

#### Declaration of Competing Interest

The authors declare that they have no known competing financial interests or personal relationships that could have appeared to influence the work reported in this paper.

#### Acknowledgements

Funding: Samantha Moratal was supported by a predoctoral contract from the Universidad Cardenal Herrera-CEU, CEU Universities (FPI CEU-UCH), and an international mobility grant from the CEU International Doctoral School (CEINDO) and Banco Santander. This research did not receive any specific grant from funding agencies in the public, commercial, or not-for-profit sectors.

#### Appendix A. Supporting information

Supplementary data associated with this article can be found in the online version at doi:10.1016/j.vetpar.2023.110050.

#### References

- Adroher, F.J., Malagón, D., Valero, A., Benítez, R., 2004. *In vitro* development of the fish parasite *Hysterothylacium aduncum* from the third larval stage recovered from a host to the third larval stage hatched from the egg. Dis. Aquat. Organ. 58, 41–45. <https://doi.org/10.3354/dao058041>.
- Adroher-Auroux, F.J., Benítez-Rodríguez, R., 2020. Anisakiasis and *Anisakis*: an underdiagnosed emerging disease and its main etiological agents. Res. Vet. Sci. 132, 535–545. <https://doi.org/10.1016/j.rvsc.2020.08.003>.
- Aibinu, I.E., Smooker, P.M., Lopata, A.L., 2019. *Anisakis* nematodes in fish and shellfish - from infection to allergies. Int. J. Parasitol. Parasites Wildl. 9, 384–393. <https://doi.org/10.1016/j.ijppaw.2019.04.007>.
- Altschul, S.F., Gish, W., Miller, W., Myers, E.W., Lipman, D.J., 1990. Basic local alignment search tool. J. Mol. Biol. 215, 403–410. [https://doi.org/10.1016/S0022-2836\(05\)80360-2](https://doi.org/10.1016/S0022-2836(05)80360-2).
- Ambros, V., 1989. A hierarchy of regulatory genes controls a larva-to-adult developmental switch in *C. elegans*. Cell 57, 49–57. [https://doi.org/10.1016/0092-8674\(89\)90171-2](https://doi.org/10.1016/0092-8674(89)90171-2).
- Ambros, V., Horvitz, H.R., 1984. Heterochronic mutants of the nematode *Caenorhabditis elegans*. Science 226, 409–416. <https://doi.org/10.1126/science.6494891>.
- Audicana, M.T., Kennedy, M.W., 2008. *Anisakis simplex*: from obscure infectious worm to inducer of immune hypersensitivity. Clin. Microbiol. Rev. 21, 360–379. <https://doi.org/10.1128/CMR.0012-07>.
- Baeza, M.L., Rodríguez, A., Matheu, V., Rubio, M., Tornero, P., De Barrio, M., Herrero, T., Santaolalla, M., Zubeldia, J.M., 2004. Characterization of allergens secreted by *Anisakis simplex* parasite: clinical relevance in comparison with somatic allergens. Clin. Exp. Allergy 34, 296–302. <https://doi.org/10.1111/j.1365-2222.2004.01883.x>.
- Bahloul, Q.Z.M., Skovgaard, A., Kania, P.W., Buchmann, K., 2013. Effects of excretory/secretory products from *Anisakis simplex* (Nematoda) on immune gene expression in rainbow trout (*Oncorhynchus mykiss*). Fish. Shellfish Immunol. 35, 734–739. <https://doi.org/10.1016/j.fsi.2013.06.007>.
- Bartie, K.L., Taslima, K., Bekaert, M., Wehner, S., Syaifudin, M., Taggart, J.B., de Verdal, H., Rosario, W., Muyalde, N., Benzie, J.A.H., McAndrew, B.J., Penman, D.J., 2020. Species composition in the Molobucus hybrid tilapia strain. Aquaculture 526, 735433. <https://doi.org/10.1016/J.AQUACULTURE.2020.735433>.

- Benazzi, M., 1982. Speciation events as evidenced in Turbellaria. In: Barigozzi, C. (Ed.), *Mechanisms of Speciation*. Alan R. Liss, New York, pp. 307–344.
- Benesch, D.P., Lafferty, K.D., Kuris, A., 2017. A life cycle database for parasitic acanthocephalans, cestodes, and nematodes. *Ecology* 98, 882. <https://doi.org/10.1002/ecy.1680>.
- Bouwknegt, M., Devleeschauwe, B., Graham, H., Robertson, L.J., van der Giessen, J., 2018. Prioritisation of foodborne parasites in Europe, 2016. *Eur. Surveill.* 23, 17–00161. <https://doi.org/10.2807/1560-7917.ES.2018.23.9.17-00161>.
- Bratley, J., Clark, K.J., 1992. Effect of temperature on egg hatching and survival of larvae of *Anisakis simplex* B (Nematoda: Ascaridoidea). *Can. J. Zool.* 70, 274–279. <https://doi.org/10.1139/z92-041>.
- Cabral-de-Mello, D.C., Marec, F., 2021. Universal fluorescence in situ hybridization (FISH) protocol for mapping repetitive DNAs in insects and other arthropods. *Mol. Genet. Genom.* 296, 513–526. <https://doi.org/10.1007/s00438-021-01765-2>.
- Carlton, P.M., Davis, R.E., Ahmed, S., 2022. Nematode chromosomes. *Genetics* 221. <https://doi.org/10.1093/genetics/iyac014>.
- Cavallero, S., Bellini, I., Pizzarelli, A., Arcà, B., D'Amelio, S., 2022. A miRNAs catalogue from third-stage larvae and extracellular vesicles of *Anisakis pegreffii* provides new clues for host-parasite interplay. *Sci. Rep.* 12, 1–13. <https://doi.org/10.1038/s41598-022-13594-3>.
- Cavallero, S., Lombardo, F., Su, X., Salvemini, M., Cantacessi, C., D'Amelio, S., 2018. Tissue-specific transcriptomes of *Anisakis simplex* (sensu stricto) and *Anisakis pegreffii* reveal potential molecular mechanisms involved in pathogenicity. *Parasit. Vectors* 11, 1–13. <https://doi.org/10.1186/s13071-017-2585-7>.
- Cheong, M.C., Wang, Z., Jaleta, T.G., Li, X., Lok, J.B., Kliever, S.A., Mangelsdorf, D.J., 2021. Identification of a nuclear receptor/coactivator developmental signaling pathway in the nematode parasite *Strongyloides stercoralis*. *Proc. Natl. Acad. Sci. U. S. A.* 118, 1–8. <https://doi.org/10.1073/pnas.2021864118>.
- Cotton, S., Donnelly, S., Robinson, M.W., Dalton, J.P., Thivierge, K., 2012. Defense peptides secreted by helminth pathogens: antimicrobial and/or immunomodulator molecules. *Front. Immunol.* 3, 1–7. <https://doi.org/10.3389/fimmu.2012.00269>.
- D'Amelio, S., Mathiopoulos, K.D., Santos, C.P., Pugachev, O.N., Webb, S.C., Picanço, M., Paggi, L., 2000. Genetic markers in ribosomal DNA for the identification of members of the genus *Anisakis* (Nematoda: Ascaridoidea) defined by polymerase-chain-reaction-based restriction fragment length polymorphism. *Int. J. Parasitol.* 30, 223–226. [https://doi.org/10.1016/S0020-7519\(99\)00178-2](https://doi.org/10.1016/S0020-7519(99)00178-2).
- Daschner, A., Pascual, C.Y., 2005. *Anisakis simplex*: sensitization and clinical allergy. *Curr. Opin. Allergy Clin. Immunol.* 5, 281–285. <https://doi.org/10.1097/01.all.0000168795.12701.fd>.
- Davey, K.G., Kan, S.P., 1968. Molting in a parasitic nematode, *Phocanema decipiens*. IV. Ecdysis and its control. *Can. J. Zool.* 46, 893–898. <https://doi.org/10.1139/z68-125>.
- Davey, J.T., 1969. The Early Development of *Contraecaeum osculatium*. *J. Helminthol.* 43, 293–298. <https://doi.org/10.1017/S0022149X00004843>.
- de Meester, N., Derycke, S., Bonte, D., Moens, T., 2011. Salinity effects on the coexistence of cryptic species: a case study on marine nematodes. *Mar. Biol.* 158, 2717–2726. <https://doi.org/10.1007/s00227-011-1769-5>.
- Doyle, S.R., 2022. Improving helminth genome resources in the post-genomic era. *Trends Parasitol.* 38, 831–840. <https://doi.org/10.1016/j.pt.2022.06.002>.
- European Food Safety Authority (EFSA) Panel on Biological Hazards (BIOHAZ), 2010. Scientific opinion on risk assessment of parasites in fishery products. *EFSA J.* 8, 1543. <https://doi.org/10.2903/j.efsa.2010.1543>.
- Fæste, C.K., Jonscher, K.R., Dooper, M.M.W.B., Egge-Jacobsen, W., Moen, A., Daschner, A., Egeas, E., Christians, U., 2014. Characterisation of potential novel allergens in the fish parasite *Anisakis simplex*. *EuPA Open Prote* 4, 140–155. <https://doi.org/10.1016/j.euprot.2014.06.006>.
- Fredensborg, B.L., Poulin, R., 2005. In vitro cultivation of *Maritrema novaezealandensis* (Microphallidae): the effect of culture medium on excystation, survival and egg production. *Parasitol. Res.* 95, 310–313. <https://doi.org/10.1007/s00436-004-1293-3>.
- Gang, S.S., Castelletto, M.L., Yang, E., Ruiz, F., Brown, T.M., Bryant, A.S., Grant, W.N., Hallem, E.A., 2020. Chemosensory mechanisms of host seeking and infectivity in skin-penetrating nematodes. *Proc. Natl. Acad. Sci. U. S. A.* 117, 17913–17923. <https://doi.org/10.1073/pnas.1909710117>.
- Giribet, G., Edgecombe, G.D., 2017. Current understanding of Ecdysozoa and its internal phylogenetic relationships. *Integr. Comp. Biol.* 57, 455–466. <https://doi.org/10.1093/icb/ixc072>.
- Glaser, R.W., 1917. Cited in: Lokwood, A. P. M., 1961. 'Ringer' solutions and some notes on the physiological basis of their ionic composition. In: *Comp Biochem Physiol*, 2, pp. 241–289. [https://doi.org/10.1016/0010-406X\(61\)90113-X](https://doi.org/10.1016/0010-406X(61)90113-X).
- Gomes, T.L., Quiazon, K.M., Itoh, N., Fujise, Y., Yoshinaga, T., 2023. Effects of temperature on eggs and larvae of *Anisakis simplex* sensu stricto and *Anisakis pegreffii* (Nematoda: Anisakidae) and its possible role on their geographic distributions. In: *Parasitol. Int.* 92, 102684. <https://doi.org/10.1016/j.parint.2022.102684>.
- Goodrich, H.B., 1916. The germ cells in *Ascaris incurva*. *J. Exp. Zool.* 21, 61–99. <https://doi.org/10.1002/jez.1400210105>.
- Harnett, W., 2014. Secretory products of helminth parasites as immunomodulators. *Mol. Biochem. Parasitol.* 195, 130–136. <https://doi.org/10.1016/j.molbiopara.2014.03.007>.
- Højgaard, D.P., 1998. Impact of temperature, salinity and light on hatching of eggs of *Anisakis simplex* (Nematoda, Anisakidae), isolated by a new method, and some remarks on survival of larvae. *Sarsia* 83, 21–28. <https://doi.org/10.1080/00364827.1998.10413666>.
- Huizinga, H.W., 1966. Studies on the life cycle and development of *Contraecaeum spiculigerum* (Rudolphi, 1809) (Ascaroidea: Heterocheilidae) from marine piscivorous birds. *J. Elisha Mitchell Sci. Soc.* 82, 181–195.
- Huizinga, H.W., 1967. The life cycle of *Contraecaeum multipapillatum* (Von Drasche 1882) Lucker, 1941 (Nematoda: Heterocheilidae). *J. Parasitol.* 53, 368–375.
- Iglesias, L., Valero, A., Benítez, R., Adroher, F.J., 2001. *In vitro* cultivation of *Anisakis simplex*: pepsin increases survival and molting from fourth larval to adult stage. *Parasitology* 123, 285–291. <https://doi.org/10.1017/S0031182001008423>.
- International Helminth Genomes Consortium, 2019. Comparative genomics of the major parasitic worms. *Nat. Genet.* 51, 163–174. <https://doi.org/10.1038/s41588-018-0262-1>.
- Irlé, T., Schierenberg, E., 2002. Developmental potential of fused *Caenorhabditis elegans* oocytes: generation of giant and twin embryos. *Dev. Genes Evol.* 212, 257–266. <https://doi.org/10.1007/s00427-002-0232-5>.
- Jasmer, D.P., Rosa, B., Tyagi, R., Mitreva, M., 2019. Omics driven understanding of the intestines of parasitic nematodes. *Front. Genet.* 10, 1–17. <https://doi.org/10.3389/fgene.2019.00652>.
- Kassambara, A., 2023. rstatix: pipe-Friendly framework for basic statistical tests. R package version 0.7.2 [WWW Document]. URL (<https://cran.r-project.org/web/packages/rstatix/>) (Accessed 20 February 23).
- Krysko, D.V., Agostinis, P., Krysko, O., Garg, A.D., Bachert, C., Lambrecht, B.N., Vandenabeele, P., 2011. Emerging role of damage-associated molecular patterns derived from mitochondria in inflammation. *Trends Immunol.* 32, 157–164. <https://doi.org/10.1016/j.it.2011.01.005>.
- Kumar, S., Stecher, G., Li, M., Knyaz, C., Tamura, K., 2018. MEGA X: molecular evolutionary genetics analysis across computing platforms. *Mol. Biol. Evol.* 35, 1547–1549. <https://doi.org/10.1093/molbev/msy096>.
- Lazetić, V., Fay, D.S., 2017. Molting in *C. elegans*. *Worm* 6, e1330246. <https://doi.org/10.1080/21624054.2017.1330246>.
- Le Verge-Serandour, M., Turlier, H., 2021. A hydro-osmotic coarsening theory of biological cavity formation. *PLoS Comput. Biol.* 17, e1009333. <https://doi.org/10.1371/journal.pcbi.1009333>.
- Lee, J.D., Chung, L.Y., Lin, R.J., Wang, J.J., Tu, H.P., Yen, C.M., 2017. Excretory/secretory proteases and mechanical movement of *Anisakis pegreffii* infective larvae in the penetration of BALB/c mice gastrointestinal. *Kaohsiung J. Med. Sci.* 33, 594–601. <https://doi.org/10.1016/j.kjms.2017.08.002>.
- Leuckart, R., 1876. Die menschlichen Parasiten und die von ihnen herrührenden Krankheiten: vol. 2. CF Winter'sche Verlagshandlung, Leipzig.
- Lin, K.W., Yan, J., 2008. Endings in the middle: current knowledge of interstitial telomeric sequences. *Mutat. Res.* 658, 95–110. <https://doi.org/10.1016/j.mrrev.2007.08.006>.
- Llarena-Reino, M., Abollo, E., Regueira, M., Rodríguez, H., Pascual, S., 2015. Horizon scanning for management of emerging parasitic infections in fishery products. *Food Control* 49, 49–58. <https://doi.org/10.1016/j.foodcont.2013.09.005>.
- Lloyd, M.M., Poulin, R., 2011. *In vitro* culture of marine trematodes from their snail first intermediate host. *Exp. Parasitol.* 129, 101–106. <https://doi.org/10.1016/j.exppara.2011.07.009>.
- Lyamzaev, K.G., Zinovkin, R.A., Chernyak, B.V., 2022. Extrusion of mitochondria: garbage clearance or cell-cell communication signals. *J. Cell. Physiol.* 237, 2345–2356. <https://doi.org/10.1002/jcp.30711>.
- Marcogliese, D.J., 1997. Fecundity of sealworm (*Pseudoterranova decipiens*) infecting grey seals (*Halichoerus grypus*) in the Gulf of St. Lawrence, Canada: lack of density-dependent effects. *Int. J. Parasitol.* 27, 1401–1409. [https://doi.org/10.1016/S0020-7519\(97\)00129-X](https://doi.org/10.1016/S0020-7519(97)00129-X).
- McClelland, G., Ronald, K., 1974. *In vitro* development of the nematode *Contraecaeum osculatium* Rudolphi 1802 (Nematoda: Anisakinae). *Can. J. Zool.* 52, 847–855. <https://doi.org/10.1139/z74-114>.
- McClelland, G., 1980. *Phocanema decipiens*: growth, reproduction, and survival in seals. *Exp. Parasitol.* 49, 175–187. [https://doi.org/10.1016/0014-4894\(80\)90115-0](https://doi.org/10.1016/0014-4894(80)90115-0).
- McSorley, H.J., Hewitson, J.P., Maizels, R.M., 2013. Immunomodulation by helminth parasites: defining mechanisms and mediators. *Int. J. Parasitol.* 43, 301–310. <https://doi.org/10.1016/j.ijpara.2012.11.011>.
- Measures, L.N., 1996. Effect of temperature and salinity on development and survival of eggs and free-living larvae of sealworm (*Pseudoterranova decipiens*). *Can. J. Fish. Aquat. Sci.* 53, 2804–2807. <https://doi.org/10.1139/cjfas-53-12-2804>.
- Melentijevic, I., Toth, M.L., Arnold, M.L., Guasp, R.J., Harinath, G., Nguyen, K.C., Taub, D., Parker, J.A., Neri, C., Gabel, C.V., Hall, D.H., Driscoll, M., 2017. *C. elegans* neurons jettison protein aggregates and mitochondria under neurotoxic stress. *Nature* 542, 367–371. <https://doi.org/10.1038/nature21362>.
- Messina, C.M., Pizzo, F., Santulli, A., Bušelić, I., Boban, M., Orhanović, S., Mladineo, I., 2016. *Anisakis pegreffii* (Nematoda: Anisakidae) products modulate oxidative stress and apoptosis-related biomarkers in human cell lines. *Parasit. Vectors* 9, 1–10. <https://doi.org/10.1186/s13071-016-1895-5>.
- Mladineo, I., Charouli, A., Jelić, F., Chakraborty, A., Hrbar, J., 2023. *In vitro* culture of the zoonotic nematode *Anisakis pegreffii* (Nematoda, Anisakidae). *Parasit. Vectors* 16, 51. <https://doi.org/10.1186/s13071-022-05629-5>.
- Müller, F., Wicky, C., Spicher, A., Tobler, H., 1991. New telomere formation after developmentally regulated chromosomal breakage during the process of chromatin diminution in *Ascaris lumbricoides*. *Cell* 67, 815–822. [https://doi.org/10.1016/0092-8674\(91\)90076-B](https://doi.org/10.1016/0092-8674(91)90076-B).
- Nadler, S.A., Hudspeth, D.S.S., 2000. Phylogeny of the Ascaridoidea (Nematoda: Ascaridida) based on three genes and morphology: hypotheses of structural and sequence evolution. *J. Parasitol.* 86, 380–393. [https://doi.org/10.1645/0022-3395\(2000\)086\[0380:POTANA\]2.0.CO;2](https://doi.org/10.1645/0022-3395(2000)086[0380:POTANA]2.0.CO;2).
- Nielsen, M.K., Wang, J., Davis, R., Bellow, J.L., Lyons, E.T., Lear, T.L., Goday, C., 2014. *Parascaris univalens* - a victim of large-scale misidentification? *Parasitol. Res.* 113, 4485–4490. <https://doi.org/10.1007/s00436-014-4135-y>.
- Orosová, M., Marková, A., Provozničková, I., Oros, M., Radačovská, A., Čadková, Z., Marec, F., 2021. Molecular cytogenetic analysis of a triploid population of the

- human broad tapeworm, *Dibothriocephalus latus* (Diphyllobothriidae). Parasitology 148, 787–797. <https://doi.org/10.1017/S0031182021000408>.
- Page, A.P., Stepek, G., Winter, A.D., Pertab, D., 2014. Enzymology of the nematode cuticle: a potential drug target. Int. J. Parasitol. Drugs Drug Resist 4, 133–141. <https://doi.org/10.1016/j.ijpddr.2014.05.003>.
- Podbielski, L., Hiebenthal, C., Hajati, M.C., Bock, C., Bleich, M., Melzner, F., 2022. Capacity for cellular osmoregulation defines critical salinity of marine invertebrates at low salinity. Front. Mar. Sci. 9, 1–19. <https://doi.org/10.3389/fmars.2022.898364>.
- R Core Team, 2021. R: a language and environment for statistical computing. R Foundation for Statistical Computing, Vienna, Austria [WWW document]. URL (<https://www.R-project.org/>) (Accessed 8 February 23).
- Roca-Geronès, X., Segovia, M., Godínez-González, C., Fisa, R., Montoliu, I., 2020. *Anisakis* and *Hysterothylacium* species in Mediterranean and North-East Atlantic fishes commonly consumed in Spain: epidemiological, molecular and morphometric discriminant analysis. Int. J. Food Microbiol 325, 108642. <https://doi.org/10.1016/j.ijfoodmicro.2020.108642>.
- Rocco, L., Costagliola, D., Stingo, V., 2001. TTAGGG<sub>n</sub> telomeric sequence in selachian chromosomes. Heredity 87, 583–588. <https://doi.org/10.1046/j.1365-2540.2001.00945.x>.
- Ronquist, F., Teslenko, M., Van Der Mark, P., Ayres, D.L., Darling, A., Höhna, S., Larget, B., Liu, L., Suchard, M.A., Huelsenbeck, J.P., 2012. MrBayes 3.2: efficient bayesian phylogenetic inference and model choice across a large model space. Syst. Biol. 61, 539–542. <https://doi.org/10.1093/sysbio/sys029>.
- Sahara, K., Marec, F., Traut, W., 1999. TTAGG telomeric repeats in chromosomes of some insects and other arthropods. Chromosom. Res 7, 449–460. <https://doi.org/10.1023/A:1009297729547>.
- Sarhan, M., Land, W.G., Tonnus, W., Hugo, C.P., Linkermann, A., 2018. Origin and consequences of necroinflammation. Physiol. Rev. 98, 727–780. <https://doi.org/10.1152/physrev.00041.2016>.
- Schierenberg, E., Sommer, R.J., 2014. Chapter 2: Reproduction and development in Nematodes. In: Schmidt-Rhaesa, A. (Ed.), Gastrotricha, Cycloneuralia and Gnathifera. Volume 2: Nematoda. Walter de Gruyter GmbH, Berlin/Boston, pp. 61–108.
- Schulze, J., Schierenberg, E., 2011. Evolution of embryonic development in nematodes. EvoDevo 2, 18. <https://doi.org/10.1186/2041-9139-2-18>.
- Smith, J.W., 1988. An electronic method for estimating the vaginal and uterine egg content of nematodes, with special reference to ascaridoids. Can. J. Zool. 66, 2253–2254. <https://doi.org/10.1139/z88-333>.
- Smith, J.W., 1983. *Anisakis Simplex* (Rudolphi, 1809, Det. Krabbe, 1878) (Nematoda: Ascaridoidea): morphology and morphometry of larvae from euphausiids and fish, and a review of the life-history and ecology. J. Helminthol. 57, 205–224. <https://doi.org/10.1017/S0022149X00009512>.
- Starling, J.A., Maule, J., Hastie, N.D., Allshire, R.C., 1990. Extensive telomere repeat arrays in mouse are hypervariable. Nucleic Acids Res 18, 6881–6888. <https://doi.org/10.1093/nar/18.23.6881>.
- Tanveer, A.S., Ahmad, F., Bashir, A.S., Mohi Ud Din Sofi, O., Fazili, K. M., 2015. Cromosomas y citogenética de helmintos (Turbellaria, Trematoda, Cestoda, Nematodacanthocephala). Neotrop. Helminthol. 9. <https://doi.org/10.24039/rnh201591787>.
- Thomas, L.J., 1937. On the life cycle of *Contracaecum spiculigerum* (Rud.). J. Parasitol. 23, 429–431.
- Traut, W., Szczepanowski, M., Vítková, M., Opitz, C., Marec, F., Zrzavý, J., 2007. The telomere repeat motif of basal Metazoa. Chromosom. Res 15, 371–382. <https://doi.org/10.1007/s10577-007-1132-3>.
- Trumbić, Z., Hrabar, J., Palevich, N., Carbone, V., Mladineo, I., 2021. Molecular and evolutionary basis for survival, its failure, and virulence factors of the zoonotic nematode *Anisakis pegreffii*. Genomics 113, 2891–2905. <https://doi.org/10.1016/j.ygeno.2021.06.032>.
- Ugland, K.I., Strømnes, E., Berland, B., Aspholm, P.E., 2004. Growth, fecundity and sex ratio of adult whaleworm (*Anisakis simplex*; Nematoda, Ascaridoidea, Anisakidae) in three whale species from the North-East Atlantic. Parasitol. Res. 92, 484–489. <https://doi.org/10.1007/s00436-003-1065-5>.
- Valles-Vega, I., Molina-Fernández, D., Benítez, R., Hernández-Trujillo, S., Adroher, F.J., 2017. Early development and life cycle of *Contracaecum multipapillatum* from a brown pelican *Pelecanus occidentalis* in the Gulf of California, Mexico. Dis. Aquat. Organ. 125, 167–178. <https://doi.org/10.3354/dao03147>.
- Van Mai, H., Fotedar, R., 2018. Haemolymph constituents and osmolality as functions of moult stage, body weight, and feeding status in marron, *Cherax cainii* (Austin and Ryan, 2002) and yabbies, *Cherax destructor* (Clark, 1936). Saudi J. Biol. Sci. 25, 689–696. <https://doi.org/10.1016/j.sjbs.2016.03.007>.
- Walton, A.C., 1924. Studies on nematodes gamatogenesis. Zeitschrift für Zellen- und Gewebelehre, Berlin.
- Walton, A.C., 1940. Gametogenesis. In: Chitwood, B.G., Chitwood, M.B. (Eds.), An Introduction to Nematology. Section II. Babylon, New York, pp. 205–215.
- Wickham, H., 2016. ggplot2: elegant Graphics for Data Analysis. Springer-Verlag, New York.
- Wolpert, L., Tickle, C., Martínez Arias, A., 2015. Principles of Development. Oxford University Press, USA.
- Xie, Y., Zhang, L., 2022. Transcriptomic and proteomic analysis of marine nematode *Litoditis marina* acclimated to different salinities. Genes 13, 651. <https://doi.org/10.3390/genes13040651>.
- Zhang, Q., Raoof, M., Chen, Y., Sumi, Y., Sursal, T., Junger, W., Brohi, K., Itagaki, K., Hauser, C.J., 2010. Circulating mitochondrial DAMPs cause inflammatory responses to injury. Nature 464, 104–107. <https://doi.org/10.1038/nature08780>.